Advanced Sciences and Technology Journal

ASTJ vol. 1 (2024) 1008
10.21608/astj.2024.338750.1008
https://astj.journals.ekb.eg/

Studying the Effect of RC Slab Corrosion on Punching Behavior Using Artificial Neural Networks

Ahmed M. Gomaa [a,b*], Ehab M. Lotfy[c], Sherif A. Khafaga[d], Sally Hosny[c], Manar A. Ahmed[c]

[a]*Department of Construction and Building Engineering, Faculty of Engineering and Technology, Egyptian Chinese University, Cairo, Egypt*
[b]*Department of Civil Engineering, The Higher Institute of Engineering and Technology Fifth Settlement, Egypt.*
[c]*Department of Civil Engineering, Faculty of Engineering, Suez Canal University, Ismailia, Egypt.*
[d]*Building Materials Research and Quality Control Institute, Housing & Building National Research Center (HBRC), Cairo, Egypt*

[*]*Ahmed.MahmoudAbdEl-Khalek@ecu.edu.eg*

ARTICLEINFO

Article history:
Received 23 November 2024
Revised 10 December 2024
Accepted 12 December 2024
Available online 13 December 2024

Handling Editor: Prof. Dr. Mohamed Talaat Moustafa

Keywords:
RC slab-column joint
punching shear capacity
corrosion
artificial neural network
parameters interaction effect

ABSTRACT

In this paper, the Punching Shear (PS) behavior of RC Slab-Column Joints (SCJs) exposed to rebar corrosion is modeled using an Artificial Neural Network (ANN). A total of 629 experimental and numerical datasets were used to develop the ANN model. Eight influencing parameters were considered as the input variables in the network namely, column cross-sectional area, effective depth of the slab, compressive strength of concrete, span-to-depth ratio, reinforcement ratio, column dimension, yield strength of steel, and corrosion degree. The punching shear capacity and the ultimate deflection were considered as the output variables. A graphical user interface was developed as a practical tool for predicting the PS behavior of corroded RC slab-column joints. The developed ANN model was compared with two empirical models from the literature. The results proved the efficiency of the proposed ANN model in predicting the PS behavior of corroded RC SCJs for different slab and column geometries, material properties, reinforcement ratios, and corrosion ratios. Additionally, the proposed ANN model was compared with the design equations of two codes, the latter yielded unsafe predictions for the PS capacity of RC slab-column joints in the event of corrosion. Furthermore, the proposed ANN model was utilized in carrying out parametric study to assess the effect of the different parameters on the PS behavior of corroded RC SCJs. The ANN model proved to have the advantage of its simplicity in application compared with conventional methods such as experimental tests and finite element modeling, which are cumbersome and expensive.

1. Introduction

RC flat slab system provides more clear space, increases architectural design flexibility, reduces construction time and cost, and makes construction easier [1], [2]. However, the punching shear is crucial in RC flat slab design[3], as the punching failure is fragile and sudden and could lead to a catastrophic progressive collapse of the entire structure. When the slab is exposed to extensive punching force, substantial shear stresses emerge in the area around the slab-column joint followed by diagonal cracks that end in the formation of a cutout cone around the column[4], [5].

A wide range of experimental studies has been carried out to investigate the punching shear behavior of slab-column systems. Earlier research primarily concentrated on examining the influence of various parameters, including column dimensions, slab dimensions, loaded areas, support and loading conditions, concrete compressive strength, reinforcement yield strength, reinforcement ratio, and reinforcement arrangement, on the punching shear behavior of reinforced concrete (RC) slabs. Based on the experimental findings, several mechanically based models have been developed.

Kinnunen and Nylander [6]–[8] analyzed the experimental outcomes of circular slab-to-circular column connections and developed the sector model, which is among the most widely recognized mechanical models for predicting punching shear in slabs. Later, Broms introduced a refined model that incorporated the size effect, enabling the determination of the ultimate crack angle in slabs and mitigating the punching failure mode in flat slabs [9]. Building on the shear stress model introduced by Stasio et al. [10], Moe proposed a more efficient and widely applicable model [11]. This model later became the theoretical foundation for standards such as GB 50010-2010 [12] and ACI 318-19. Muttoni proposed the critical shear crack theory after examining the influence of aggregate size and analyzing the critical cracks in slab-column joints (SCJs) [13].

Wu et al. introduced a prediction model grounded in the modified compression field theory, validating its effectiveness through extensive experimental data [14]. Chetchotisak et al. devised a prediction model for the punching shear strength of RC slabs through regression analysis of experimental data [15].

Experimental studies provided good insight into the behavior of RC slabs in punching and created an intense source of data as well. However, it has been proven that both mechanical-based and experimental models often face challenges to predict accurately[16]–[18]. Several design codes and empirical models for estimating PS capacity were developed by statistically fitting experimental data to empirical models [15], [19]–[23]. These empirical equations are based on the experimental tests performed at the time of developing such equations. Therefore, these models only took into account the design parameters examined in the tests, which varied between test programs and depended on the amount and characteristics of the experimental data. In addition, any potential interaction between parameters was often not considered in the statistical fitting of the test data. Some of these equations can no longer provide accurate predictions. Therefore, concerns have been raised about the accuracy of these equations in PS predictions, specifically for slabs with different characteristics such as corrosion events.

Artificial intelligence (AI) techniques are rapidly emerging as a prominent research area, gaining significant interest across various engineering disciplines. Prior applications of AI models have shown that artificial neural network (ANN) models can effectively establish a strong correlation between input and output parameters for complex challenges in structural engineering [24]–[26]. A review of prior literature revealed that artificial neural networks (ANNs) possess the ability to adaptively learn from experience and derive functions suited to specific objectives [15], [19]–[23]. The primary benefit of an ANN model over traditional modeling methods is its capacity to effectively capture complex and nonlinear relationships among system parameters without needing to assume the nature of the

input-output relationships in advance. Additionally, it is generally more user-friendly than conventional techniques such as experimental studies and finite element analysis.

Reviewing the literature revealed that no study has utilized the ANN approach in investigating the punching shear behavior of corroded RC slab-column joints. This paper aims to address this research gap. The proposed methodology aims to provide a simple and effective tool, compared to conventional methods, to perform a parametric study on the punching shear behavior of corroded RC slabs using ANN.

A large experimental and numerical dataset that includes both corroded and non-corroded RC SCJs has been prepared to ensure the high performance of the obtained ANN model. The experimental data was collected from relevant literature. Since most of the previous relevant experimental studies didn't consider the corrosion factor, finite element analysis was performed using ABAQUS software to obtain extensive data for a thorough learning process of the ANN. The finite element models were prepared and validated in previous research by the authors [27].

1. Methodology framework for developing the proposed ANN model

3.1. Dataset preparation

A total of 629 experimental and numerical datasets were prepared as follows:

- Experimental datasets from the literature

A total of 232 experimental datasets were extracted from the literature (The datasets are given in appendix (1)). It was concluded from previous studies [28]–[30] that column cross-sectional area, slab effective depth, concrete compressive strength, span-to-depth ratio, reinforcement ratio, column dimension, steel yield strength, and corrosion degree are the most influencing parameters on punching behavior of corroded slabs, see in Fig 1.

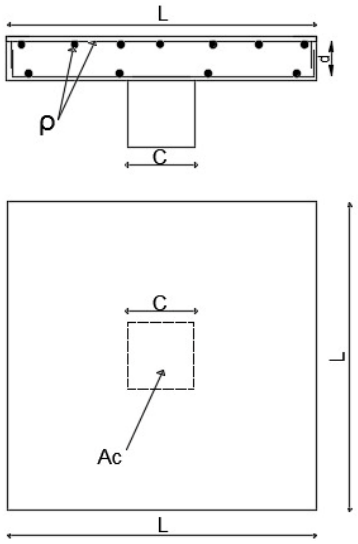

Fig. 1. Influencing parameters on punching behavior of corroded slab.

- Dataset from numerical analysis

Most of the previous experimental studies didn't consider the corrosion factor when investigating the PS capacity of RC SCJs. To overcome this shortage in the available data from the literature, numerical analysis was conducted using the finite element simulation, and ABAQUS program, and 397 datasets were extracted (The datasets are given in Appendix (1)). The finite element models used in the present numerical analysis were developed and validated in a previous work by the authors. The detailed finite element modeling can be found in [27].

3.2. Dataset description

Eight influencing parameters were considered as the input variables in the ANN, namely, column cross-sectional area, slab effective depth, reinforcement ratio, concrete compressive strength, reinforcement yield strength, span-to-depth ratio, column dimension, and corrosion ratio. While the punching shear (PS) capacity and the ultimate deflection (D_u) were considered as the output variables. The values of the considered variables were extracted from each dataset. Table 1 illustrates the minimum, maximum, standard deviation, and average values of the considered variables. The frequency distribution of the input variables in the datasets is shown in Fig. 2.

Table 1 Variables statistical description

Variable	Min	Max	Average	Std. Dev
Section area of column A_c (mm^2)	3025	342119	60299	48847
Effective slab depth d (mm)	29.7	500.0	146.4	59.7
Compressive strength of concrete (MPa)	17.5	130.1	39.4	15.7
Span-to-depth ratio L/d	1.1	20.0	6.9	2.9
Reinforcement ratio ρ (%)	0.2	2.7	1.1	0.4
Column dimension C (mm)	55	584.9	231.3	82.4
Yield strength of reinforcement f_y (Mpa)	280.0	749.0	513.9	93.1
Corrosion ratio CR (%)	0.0	30.0	10.6	10.7
Ultimate deflection D_u (mm)	0.1	46.2	4.3	4.9
Punching shear capacity (V_u) (kN)	30.5	2681.0	477.3	332.3

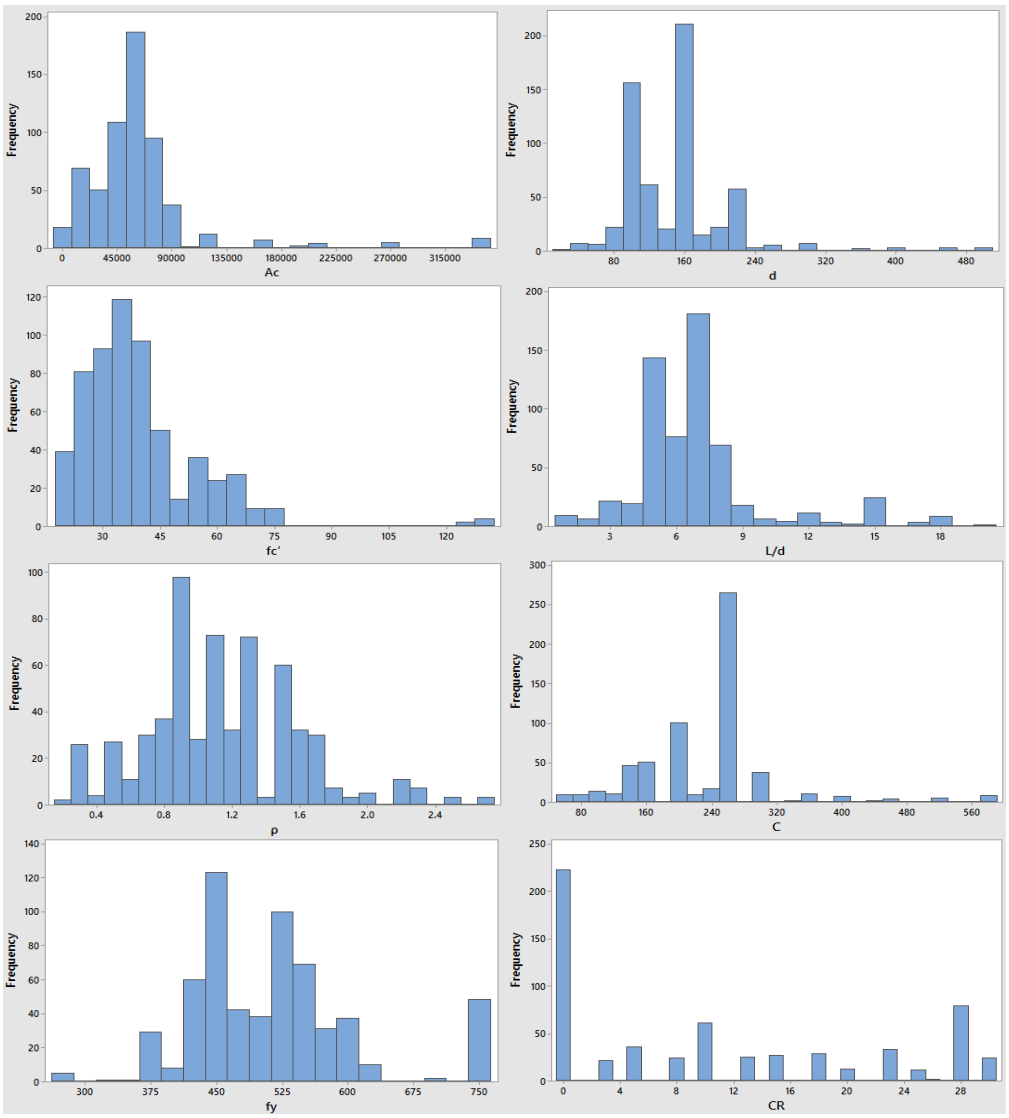

Fig. 2. Frequency distribution of the input variables.

3.3. Effective parameters and correlation

Figs. 3 and 4 show the correlation between the input and output variables in the dataset. It is evident from the literature that increasing the slab thickness, the column dimension and the cross-sectional area of the column has a positive effect on PS capacity, whereas increasing the span-to-depth ratio reduces the PS capacity of slabs. Previous research[27], [31] also confirmed that corrosion negatively affects the PS capacity, whilst increasing the flexure reinforcement ratio, the concrete compressive strength, and the reinforcement yield strength have a slight positive effect on the PS capacity of the corroded RC SCJs.

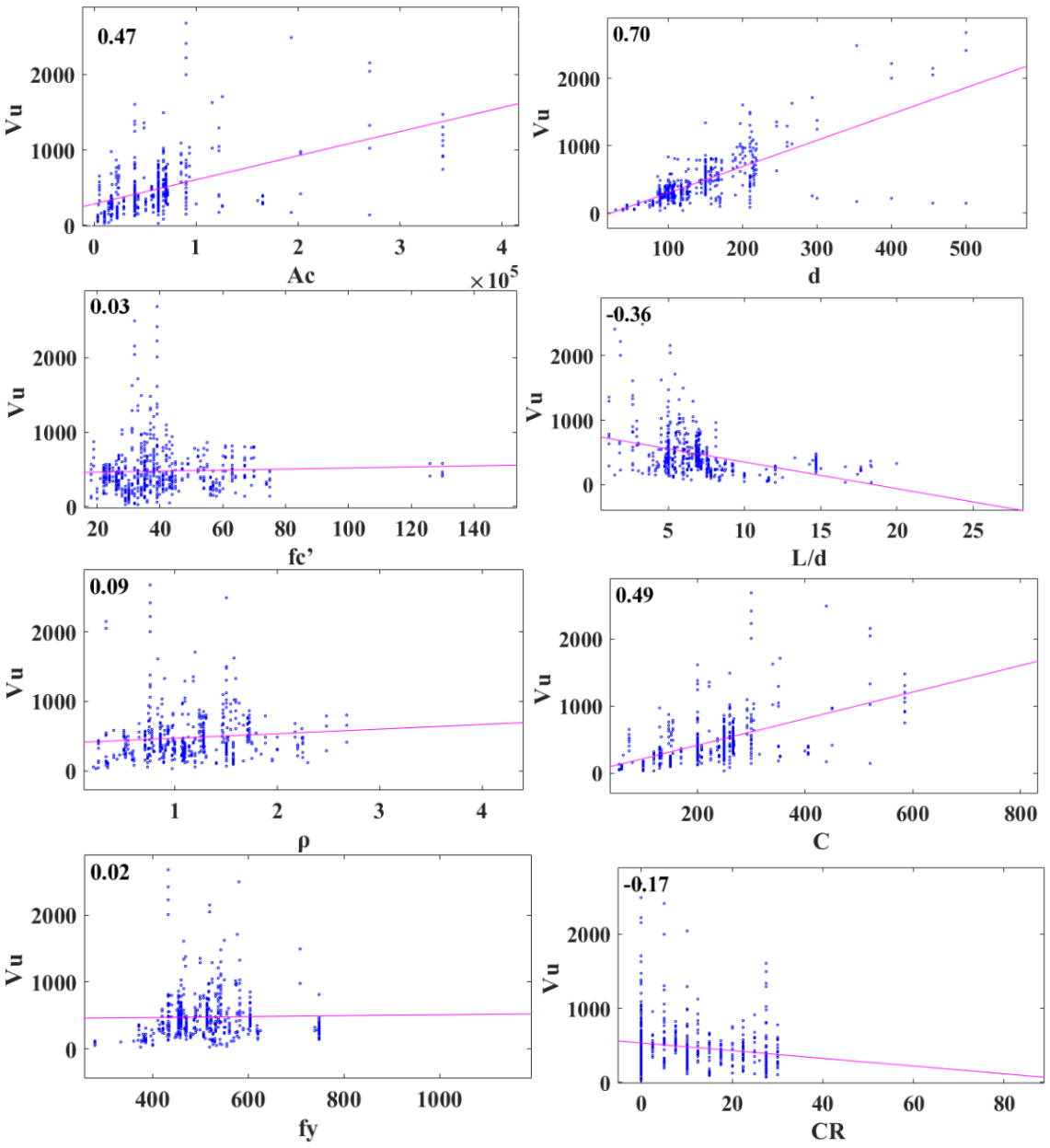

Fig. 3. Correlation plot between each input variable and the punching shear capacity in the dataset.

This result for the corroded RC SCJs is inconsistent with the verified physical resisting mechanism of the dowel action which is primarily dependent on the flexure reinforcement in the non-corroded RC SCJs. This deviation could be owing to the bond loss between the concrete and the corroded rebar surface.

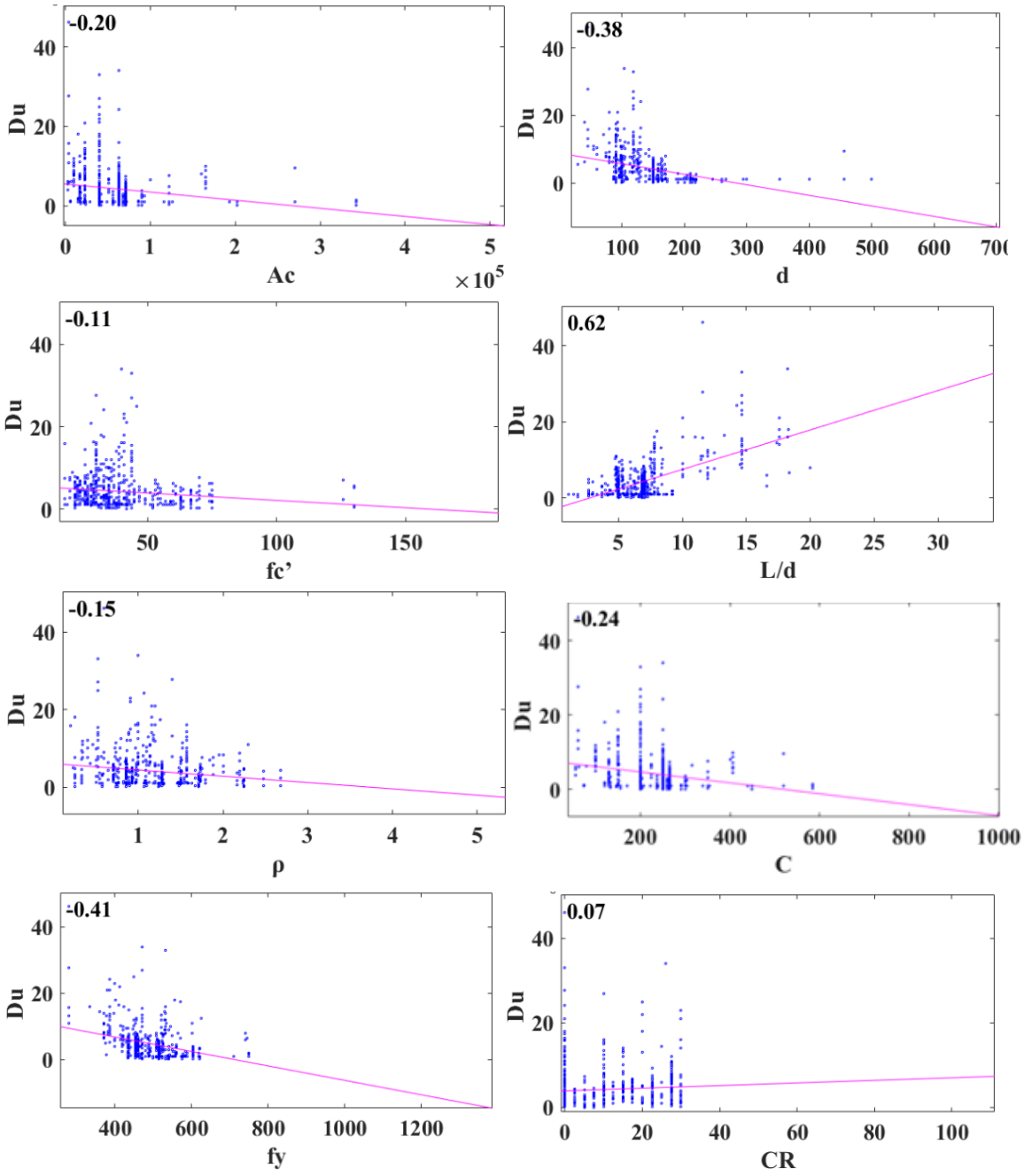

Fig. 4. Correlation plot between each input variable and the ultimate deflection in the dataset.

Although the correlation coefficients described in Figs. 3 and 4 are precise for linear relationships, but still give an indication of the relative importance of the parameters in such nonlinear relationships. It can be noticed from Fig. 3 that the punching shear capacity has a strong positive correlation with d, C, and Ac, and a negative correlation with

L/d and CR. But there is a very weak correlation with ρ and *f*y. Concerning the ultimate deflection, correlation is high with the parameters Ac, d, fc', L/d, C, ρ, and f_y, however, correlation is very low with CR, as shown in Fig.4.

3.4. Development of the ANN model

An artificial neural network (ANN) consists of multiple processing units called neurons, which are connected through links. During the training process, initial weights are assigned to these links and then adjusted by comparing predicted outputs to actual outcomes. Errors are propagated back through the network to reduce discrepancies. The weights are refined using backpropagation, a method that fine-tunes them based on the error rate from the previous training cycle. A key advantage of ANNs is their ability to identify complex relationships between input and output variables without prior knowledge of these interactions.

As shown in Equation (1), the computations within the ANN involve summing the weighted input values along with the bias from the input layer, and these results are forwarded to the neurons in the hidden layer. The tang-sigmoid function is applied in the neurons, as described in Equation (2). The outputs from the hidden layer neurons are then combined with the hidden layer's bias in another linear process using the purelin function, as indicated in Equation (3).

$$S_j = \sum_{i=1}^{n} w_{ij} x_i + b_j \quad (1)$$

$$y_j = f(S_j) = \left(1 + exp^{-(2S_j)}\right) - 1, \quad (2)$$

$$y_k = Purelin\left(\sum_{j=1}^{m} w_{jk} y_j + b_k\right), \quad (3)$$

where net_j is the weighted sum generated at the j^{th} hidden neuron; x_i is the input value from the i^{th} input neuron; w_{ij} and w_{jk} are the weights added to the hidden layer and the output layer neurons, respectively; $bias_j$ and $bias_k$ are the biases added to the hidden layer and the output layer neurons, respectively; y_j is the processed output from the j^{th} hidden neuron; y_k is the processed output from the *k*th output neuron; *n* is the number of input neurons, and m is number of neurons in the hidden layer.

In this study, the eight input parameters (Ac, d, L/d, ρ, C, fy, and CR) are represented by eight neurons in the input layer, there are two neurons in the output layer for Vu and Du. Before the training process, it is recommended to normalize the datasets in a range of (-1, 1) in order to classify the different interval values to the same scale. It is obvious that normalization enables the orthogonalization of the input vectors' components in order to prevent correlation between them and to speed up convergence during the training phase [32]. The normalized data value is given by the following equation:

$$X_{nor} = 2 \times \frac{(X - X_{min})}{(X_{max} - X_{min})} - 1 \quad (4)$$

where X represents the data sample, X_{nor}represents the normalized data sample, while X_{min} and X_{min} are the minimum and maximum values of the data for the parameter under consideration.

To train, test, and validate the neural network the datasets were divided into three sets. A subdivision with 70%, 15%, and 15% of the datasets were used for training, testing, and validating the network, respectively. The connection weights and biases were adjusted using the training set, network over-training is monitored in the validating phase while measuring the network performance is done in the testing phase. Numerous numerical optimization methods have been successfully applied to accelerate the backpropagation learning algorithm's convergence. However, the Levenberg-Marquardt (LM) method, which is a common least squares nonlinear optimization algorithm, was demonstrated by numerous researchers[33]–[35] to be particularly effective for ANN modeling. LM has a higher convergence rate and generalized performance precision than other algorithms, hence a low error would be achieved with fewer repetitions (epochs). In general, the LM algorithm is the fastest convergence algorithm for function approximation problems in networks with up to a few hundredweights. The number of neurons in the hidden layer is another important consideration in ANN training. A neural network with insufficient neurons is unable to accurately forecast the data. Like this, a neural network with huge neurons performs poorly and may experience an overtraining problem.

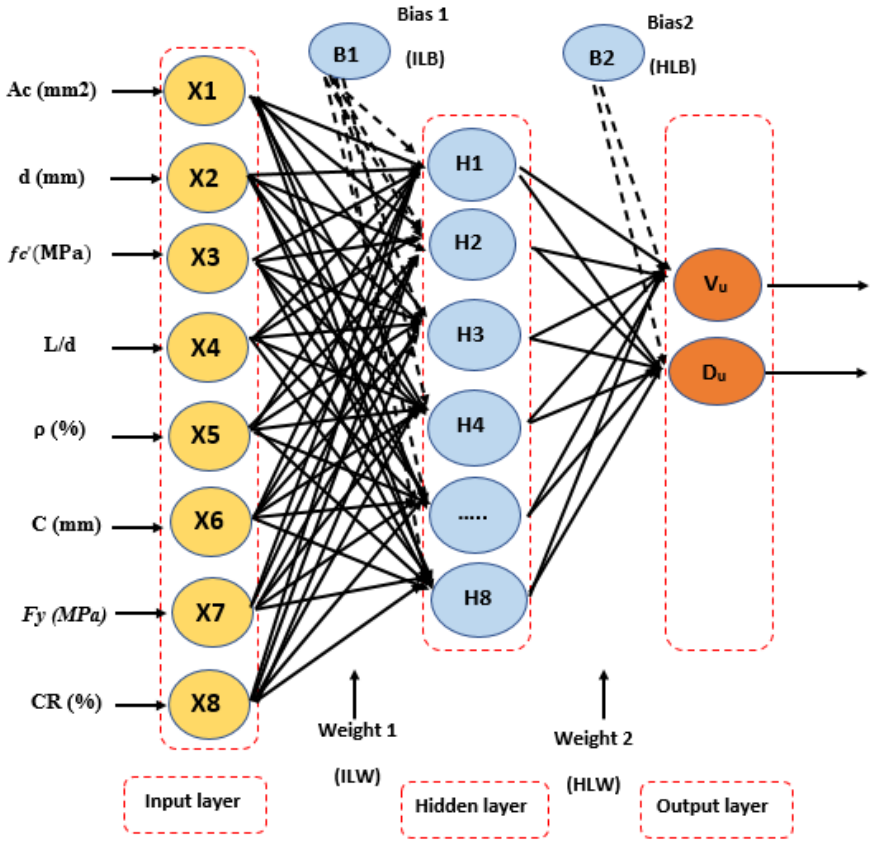

Fig. 5. The ANN model is composed of eight neurons in one hidden layer.

In this work, the optimum ANN model for the available data was determined by performing a sensitivity analysis. The LM algorithm with 8 neurons in one hidden layer showed the best performance. The final ANN model comprises an input layer with eight inputs, an output layer with two outputs, and a hidden layer with eight neurons, as shown in Fig. 5.

Fig. 6 shows the performance of the training, testing, and validation processes of the ANN model. The best validation performance was obtained at the 14th epoch. Minimum values of mean squared errors imply a reliable ANN model. Fig. 7 depicts a regression model that displays the correlation between the real values and the ANN model's predicted values. The coefficient of determination R^2 for training, testing, validation, and all data are 0.983, 0.987, 0.983, and 0.984, respectively. The overall response is with coefficients of determination close to 1, which indicates successful training. After the efficiency of the ANN is proven, the ANN model can then be frozen, and the network is now capable of computing the output values associated with new input data of corroded RC SCJs.

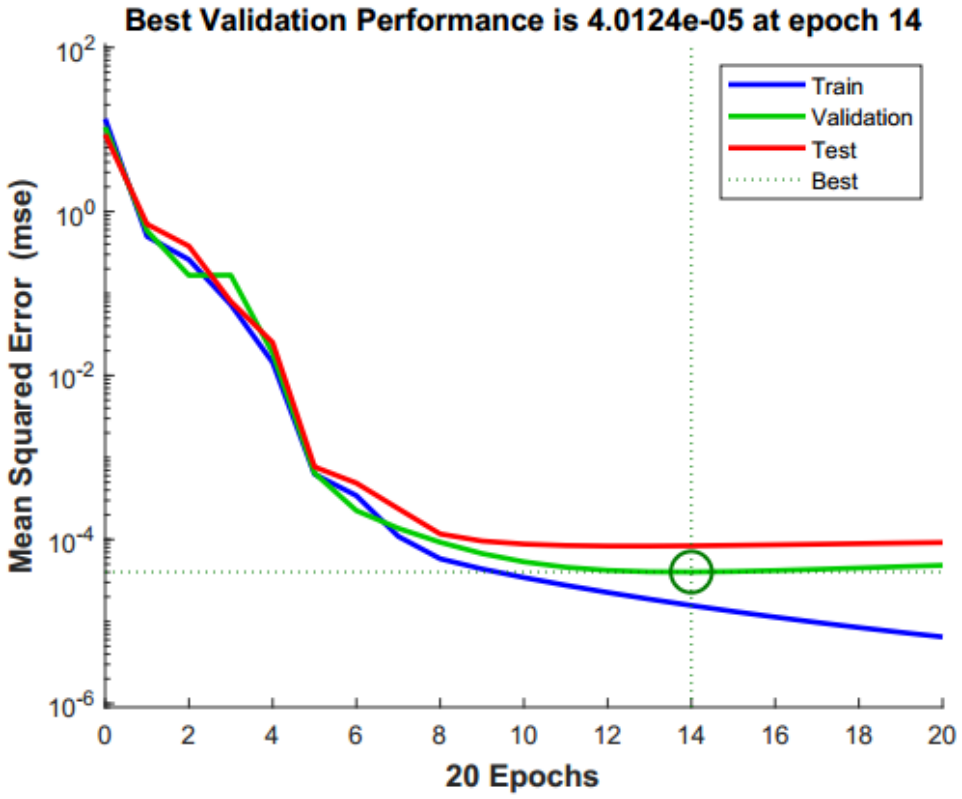

Fig. 6. Performance of the ANN training process.

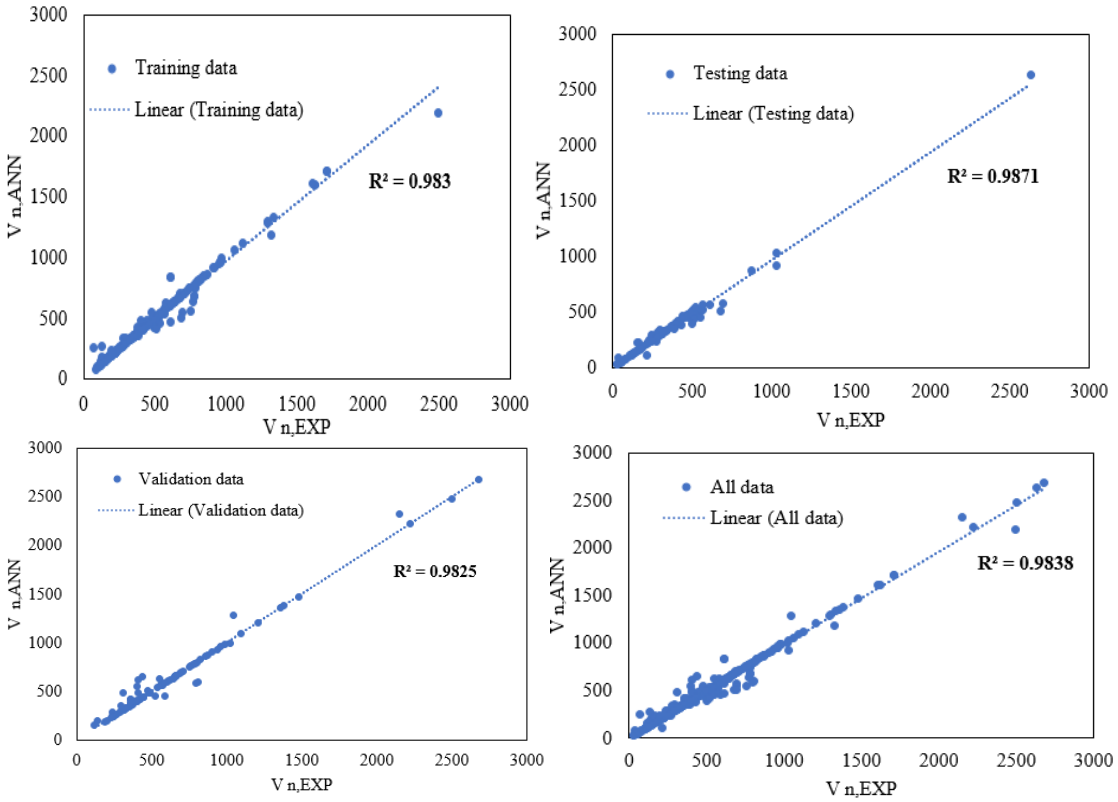

Fig. 7. Regression analysis for training, validation, testing, and all data of the ANN model.

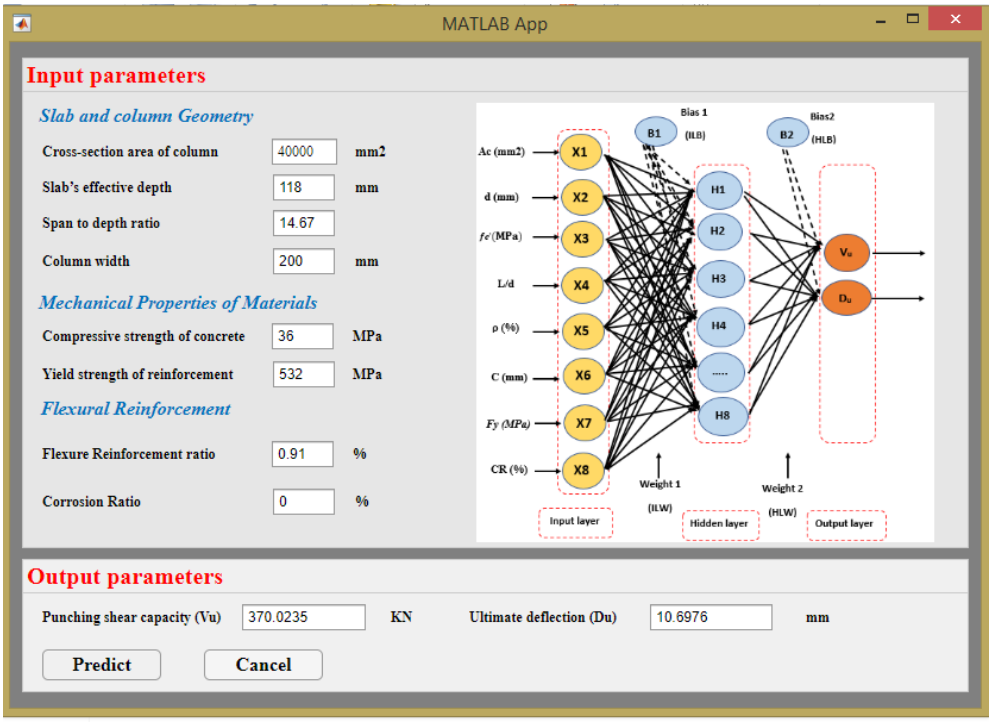

Fig. 8. Graphical user interface (GUI) for the proposed ANN model.

3.5. Development of a graphical user interface

In this study, a graphical user interface (GUI) was designed using the developed ANN model to serve as a straightforward tool for predicting the PS behavior of corroded RC SCJs. Figure 8 illustrates the GUI. The tool requires eight input variables and provides two output predictions. For accurate results, the input variables should be adjusted according to their statistical properties listed in Table 1.

3.6. Comparison between the proposed ANN model and existing models

There are a very limited number of recently developed models that consider corrosion when estimating the punching shear capacity of slab-column joints. Two of these models are presented in Table 2. The efficiency of the developed ANN model in predicting the punching shear capacity was compared with the efficiency of these two models to assess the reliability of the ANN model. The experimental specimen data of Quin et al. [31] and Ahmed et al.[27] are used for the comparison. The comparison is made through the mean value of the ratios V_t/V_c and their coefficient of variation, where V_t indicates the measured values of the experimental specimen's data and V_c indicates the predicted values, see Table 3.

Table 2: Empirical models selected for comparison.

Reference	Punching shear strength (Mpa)
Quin et al. [31]	$\frac{V_p}{\sqrt{f_c^-}b_o d} = \frac{3/4}{1+15\frac{k\psi d}{d_{g0}+d_g}}$ $k = e^{0.016CR}$
Ahmed et al.[27]	$V_p = 253.00 + 0.034 \times t_s^2 + 0.054 \times t_s \times \rho \times f_{cu} - 4.36 \times t_s - 0.024 \times CR \times t_s - 4.59 \times 10^{-5} \times t_s^3 - 0.0024 \times \rho \times f_{cu} \times S$

bo Is the critical section perimeter location, d is the effective depth of the slab, fc' is the concrete compressive strength, f_{cu} is the concrete cubic compressive strength, ts is slab thickness, CR is the corrosion ratio, S is supporting distance, ρ is the flexural reinforcement ratio of the critical section, ψ is the rotation of the slab outside the column region, d_{g0} is a reference size equal to 16 mm, d_g is the maximum aggregate size, K is a magnification factor.

Fig. 9 shows a comparison between the proposed ANN model and the models of Quin et al. [31] and Ahmed et al.[27]. The mean value of the ratios Vt/Vc and their coefficient of variation for the ANN model are 0.99 and 0.06, respectively. For Quin et al.[31] are 0.98 and 0.06, respectively, and for Ahmed et al.[27] are 1.04 and 0.12, respectively. These statistical measurements indicate that the proposed model reliably predicts the PS capacity of the tested slabs. It is worth mentioning that the prediction model of Ahmed et al.[27] is more conservative compared to the proposed ANN model and Quin et al. [31] models.

Table 3: Ratios between measured and predicted values for the ANN model and empirical models.

Ref	Specimen code	Quin et al. [31] Vt/Vc	Ahmed et al.[27] Vt/Vc	ANN model Vt/Vc
Quin et al. [31]	S1-0	1.01	1.14	1.06
	S1-10	1.05	1.10	1.09
	S1-20	1.03	1.10	1.01
	S1-30	1.04	1.21	1.03
	S2-0	0.97	0.96	0.94
	S2-10	0.98	0.96	0.93
	S2-20	0.94	0.95	0.92
	S2-30	1.03	1.08	1.06
	S3-0	0.99	1.09	1.04
	S310	0.97	1.03	1.03
	S3-20	1.04	1.12	1.02
	S3-30	1.07	1.24	1.04
Ahmed et al.[27]	S-N	0.9	0.99	0.98
	S-L	0.92	0.94	0.96
	S-M	0.9	0.88	0.92
	S-H	0.91	0.79	0.93
	Mean	0.98	1.04	0.99
	COV	0.06	0.12	0.06

Note: V_t indicates the values from the experimental specimen's data [27,28]; V_c indicates the predicted values.

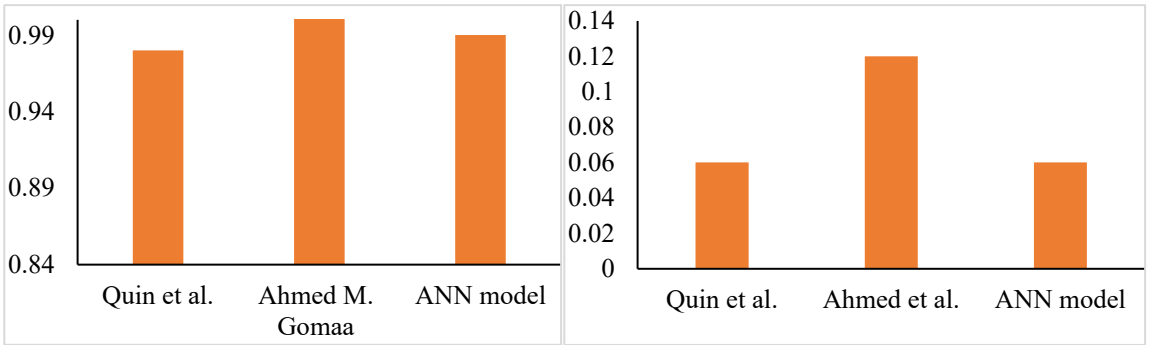

Fig. 9. Comparison between the proposed ANN model and empirical models' predictions.

3.7. Assessment of the requirements of codes in the event of corrosion

Throughout the past decades, a variety of design codes of provisions have been offered for reinforced concrete slabs subject to punching shear. The design equations for predicting the PS capacity of RC SCJs from two codes (namely, CSA 23.3–14 [36] and ACI 318-19 are displayed in Table 4. The values predicted by these equations were compared with the prediction of the proposed ANN model to assess the validity of the available code design equations in the event of corrosion. The comparison is made through the mean value of the ratios Vt/Vc and their coefficient of variation as given in Table 5. Reviewing Fig. 10 shows that the PS capacity predicted by the available code's equations is much higher than the experimental values of the corroded RC SCJ. This is obviously because the equations available

in the codes do not take corrosion into account. In contrast, the proposed ANN accurately predicts the PS behavior of the tested slabs.

Table 4: Equations of codes selected for comparison.

Reference	Punching shear strength (Mpa)	Symbols
ACI 318–19 [37]	Minimum of $V_c = \frac{1}{12}\ (1 + \frac{4}{\beta})\lambda s\lambda\sqrt{f_c^-}b_o d$ $V_c = \frac{1}{12}\ \left(\frac{\alpha s d}{b_o} + 2\right)\lambda s\lambda\sqrt{f_c^-}b_o d$ $V_c = \frac{1}{3}\lambda s\lambda\sqrt{f_c^-}b_o d$	C = size of rectangular column β is the long-to-short ratio of the column. λs is size-related effects. λ is the concrete density. αs is the column's location factor. bo is the critical section perimeter location. d is the effective depth of the slab
CSA 23.3–14 [36]	Minimum of $V_c = 0.19\ (1 + \frac{2}{\beta})\lambda\varphi_c\sqrt{f_c^-}b_o d$ $V_c = (\frac{\alpha_{sd}}{b_o} + 0.19)\lambda\varphi_c\sqrt{f_c^-}b_o d$ $V_c = 0.38\lambda\varphi_c\sqrt{f_c^-}b_o d$	fc' is the concrete compressive strength φc is the factor of concrete resistance ρ is the flexural reinforcement ratio of the critical section

Table 5: Ratios between measured and predicted values for the ANN model and the codes.

Ref	specimen code	ACI 318–19[42] Vt/Vc	CSA 23.3–14[43] Vt/Vc	ANN model Vt/Vc
Quin et al. [31]	S1-0	1.08	1.09	1.06
	S1-10	0.92	0.94	1.09
	S1-20	0.81	0.83	1.01
	S1-30	0.78	0.79	1.03
	S2-0	0.74	0.74	0.94
	S2-10	0.63	0.64	0.93
	S2-20	0.54	0.55	0.92
	S2-30	0.52	0.52	1.06
	S3-0	1.02	1.08	1.04
	S310	0.85	0.90	1.03
	S3-20	0.81	0.86	1.02
	S3-30	0.74	0.77	1.04
Ahmed et al.[27]	S-N	1.45	1.46	0.98
	S-L	1.30	1.31	0.96
	S-M	1.14	1.15	0.92
	S-H	0.97	0.98	0.93
	Mean	0.89	0.91	0.99
	COV	0.26	0.26	0.06

Note: V_t indicates the values from the experimental data[27,28]; V_c indicates the predicted values.

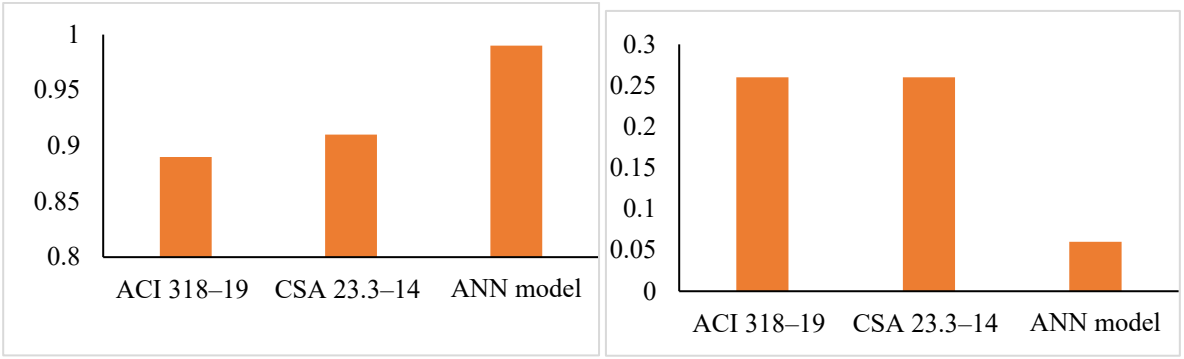

Fig. 10. Comparison between the ANN model predictions and codes.

2. Parametric study and discussion

Understanding the PS behavior of RC slabs is challenging due to the influence of many parameters involved, and it is expected to be even more difficult in the presence of corrosion. The developed ANN model was employed in a parametric study to investigate the effect of each input variable and the interaction effect between these variables on the PS behavior of the corroded reinforced concrete slabs. To achieve this, each input variable was assigned a values range within the border of the training dataset of the ANN. It is important to emphasize that for input variables outside the range of the training dataset, the ANN model cannot provide accurate predictions. The assigned values for the input variables are given in Table 6, where (L) is the lowest value, (H) is the highest value, (M) is the mean value, (LM) is the midpoint of (L) and (M), and (MH) is the midpoint of (M) and (H).

Table 6. Assigned values for each input variable.

Input variables	**L**	**ML**	**M**	**MH**	**H**
Section area of column (mm^2)	3025	42268.8	81512.5	120756	160000
The effective depth of the slab (mm)	29.7	64.775	99.85	134.925	170
Compressive strength of concrete (MPa)	18.2	25.05	31.9	38.75	45.6
Span-to-depth ratio	6.3	9.725	13.15	16.575	20
Reinforcement ratio (%)	0.2	0.725	1.25	1.775	2.3
Column dimension (mm)	55	187.477	319.955	452.432	584.91
Yield strength of reinforcement (MPa)	280	396	512	628	744
Corrosion ratio (%)	0	7.5	15	22.5	30

3.8. The relative influence of the input variables on PS capacity

Fig. 11 shows the influence of each input variable on the PS capacity. Results showed that the most influencing parameters on PS capacity of the corroded SCJs are column width, span-to-depth ratio, effective depth, and corrosion

ratio, followed by column area and reinforcement ratio, while yield strength of reinforcement and concrete compressive strength have limited effect on PS capacity. These results are consistent with other research [27], [31]. Fig. 11 shows that when (L/d) increased by 52% relative to its mean value, the PS capacity was at 69% of its value at the mean of (L/d), this is due to the size effect. When (C) increased by 83% relative to its mean value, the PS capacity enhanced by 75%, this is due to the reduction of stress concentration around the shorter side of the column. Increasing (fy) by 45% enhanced the PS capacity by only 2%, this insensitivity to reinforcement improvement could be due to the loss of integrity between concrete and corroded rebars.

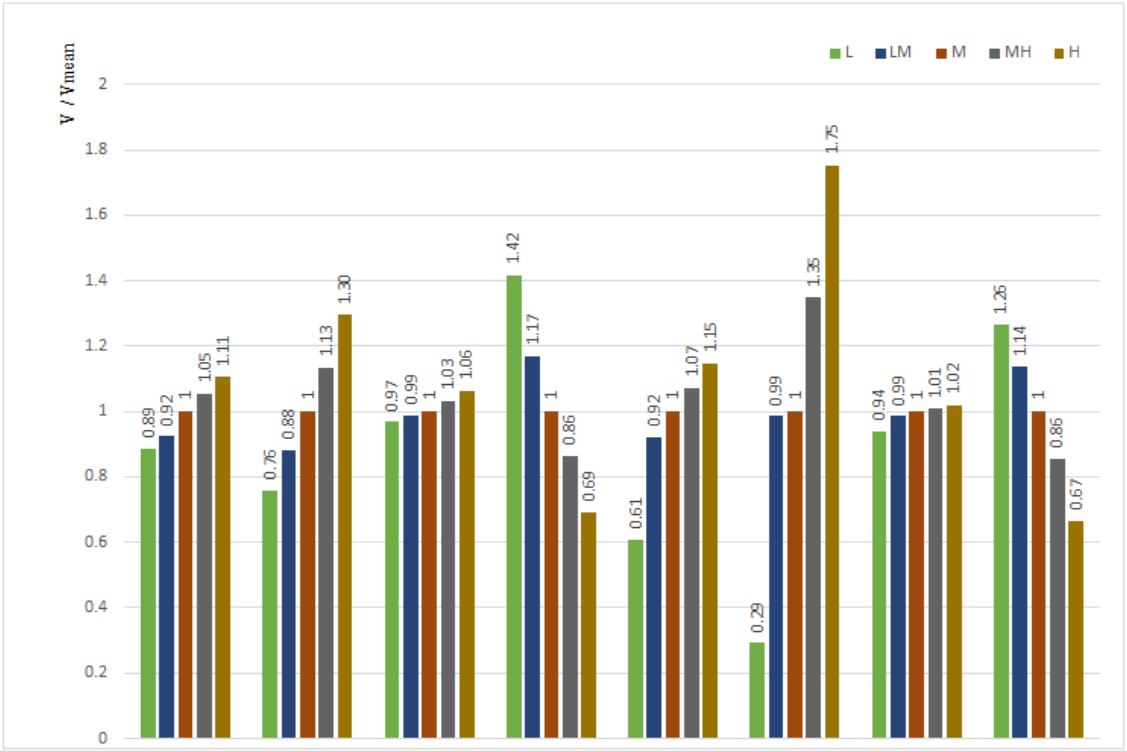

	Ac	d	fc	L/d	ρ	C	f_y	CR
(L-M)/M	-0.96	-0.70	-0.43	-0.52	-0.84	-0.83	-0.45	-1.00
(LM-M)/M	-0.48	-0.35	-0.21	-0.26	-0.42	-0.41	-0.23	-0.50
	1.00	1.00	1.00	1.00	1.00	1.00	1.00	1.00
(MH-M)/M	0.48	0.35	0.21	0.26	0.42	0.41	0.23	0.50
(H-M)/M	0.96	0.70	0.43	0.52	0.84	0.83	0.45	1.00

Fig. 11. Relative importance of the input variable's effect on PS capacity.

3.9. Interaction between effects of input variables on PS capacity.

To investigate the interaction between the input variable's effect on the PS behavior of corroded reinforced concrete slabs, 5600 datasets were obtained using the proposed ANN model to carry out this parametric study. It is worth highlighting that this huge number of datasets is a very hard task to achieve using conventional approaches such as experimental tests and finite element modeling. To illustrate the interaction between the input variables, the effect of each two input variables on PS was plotted simultaneously as shown in Figs. 12 to 19.

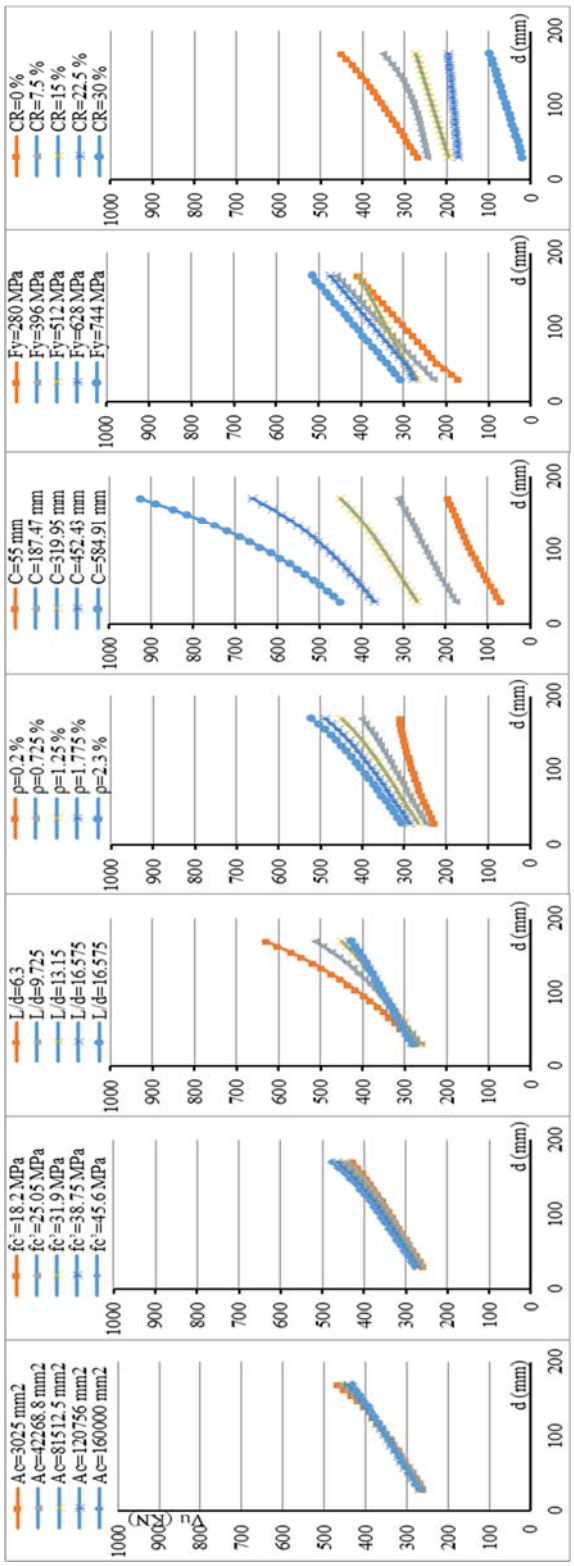

Fig. 12 Interaction effects between effective depth of corroded slabs and other input variables.

- Effect of the slab effective depth

The impact of the effective depth (d) on the punching shear capacity of corroded slabs is given in Fig. 12. Results in Fig. 12 imply that the PS capacity of corroded slabs generally increases when the effective depth increases. However, increasing the column width (C) combined with the increase of (d) is more effective than the other parameters. Additionally, Fig. 12 shows that, although the PS capacity increases with increasing the effective depth for different levels of corrosion, the rate of increasing the PS capacity is lower at higher levels of corrosion.

- Effect of section area of the column

The impact of column area (Ac) on the PS capacity of corroded slabs is shown in Fig. 13. The results of the ANN simulation analysis imply that the PS capacity of corroded slabs is not so sensitive to changing the column area. This behavior is inconsistent with the expected effect of increasing (Ac), this diversion may be due to the effect of corrosion. However, increasing (Ac) combined with increasing the column width (C) has a positive effect on PS capacity, this is owing to the reduced stress concentration around the shorter side of the column.

- Effect of concrete compressive strength

Fig. 14 shows the relationship between the PS capacity and the compressive strength of concrete (fc') at different values of the other parameters. The PS capacity marginally increases with the increase of the concrete compressive strength. In addition, increasing the concrete compressive strength accompanied by increasing the reinforcement ratio or yield strength causes minor enhancement in the PS capacity of corroded slabs. This poor sensitivity to reinforcement enhancement could be due to the bond loss between concrete and corroded rebar surfaces. However, increasing (fc') combined with increasing the column width (C) has a positive effect on PS capacity,

- Effect of span-to-depth ratio

The influence of span-to-depth ratio (L/d) on punching shear strength is presented in Fig. 15. The ANN simulation results indicate that PS capacity decreases when (L/d) increases, these results show agreement with the size effect law. However, the rate of reduction in PS decays with the increase of (L/d). In addition, the effect of (L/d) combined with the column width (C) or the effective depth (d) is more influential than the combination with other parameters.

- Effect of reinforcement ratio

Fig. 16 shows a slight improvement in the PS capacity of the corroded SCJs as the reinforcement ratio increases. Combination with the column-section area, the concrete compressive strength, or the steel yield strength causes a minor increase in PS capacity. However, a combination of reinforcement ratio with the slab's effective depth, column width, span-to-depth, or corrosion ratio noticeably affects the PS capacity.

- Effect of column width

Fig. 17 shows the effect of column width (C) on PS capacity. Increasing the column width combined with increasing the slab's effective depth improves the PS capacity significantly. Moreover, the PS capacity increases with the combined increase of the column width and the reinforcement ratio. However, the rate of increasing the PS with increasing the column width declines for higher degrees of corrosion.

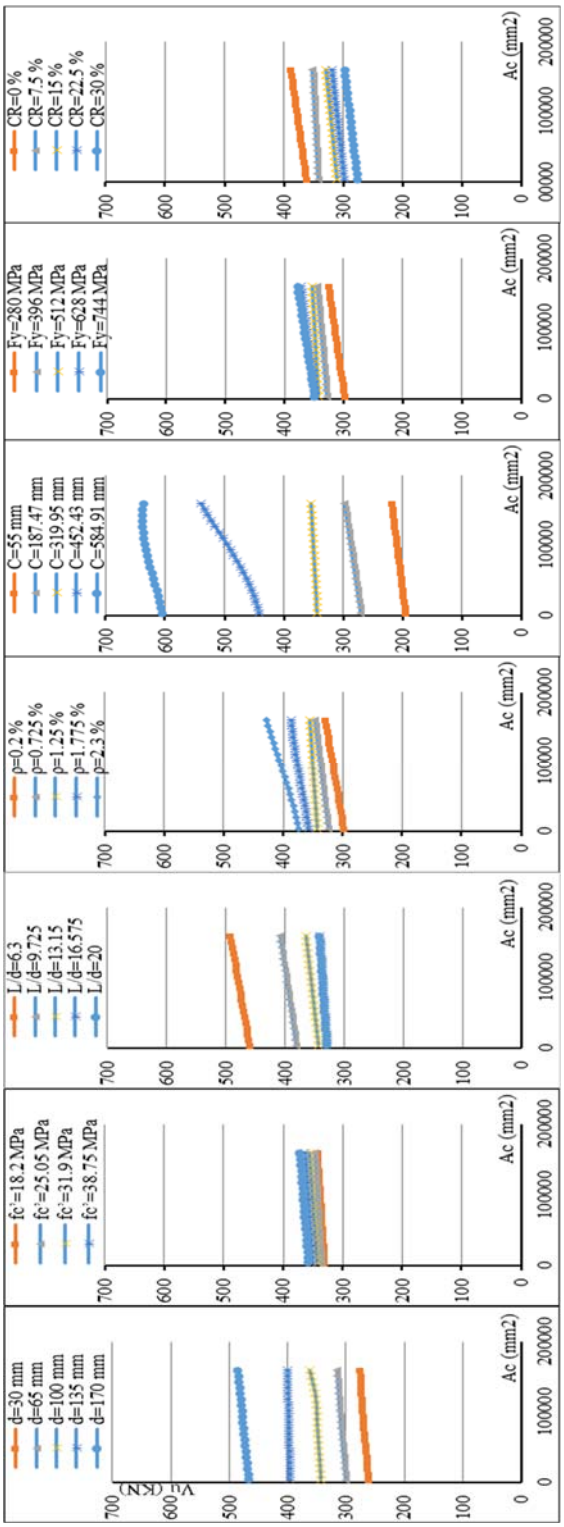

Fig. 13 Interaction effects between column area and other input variables.

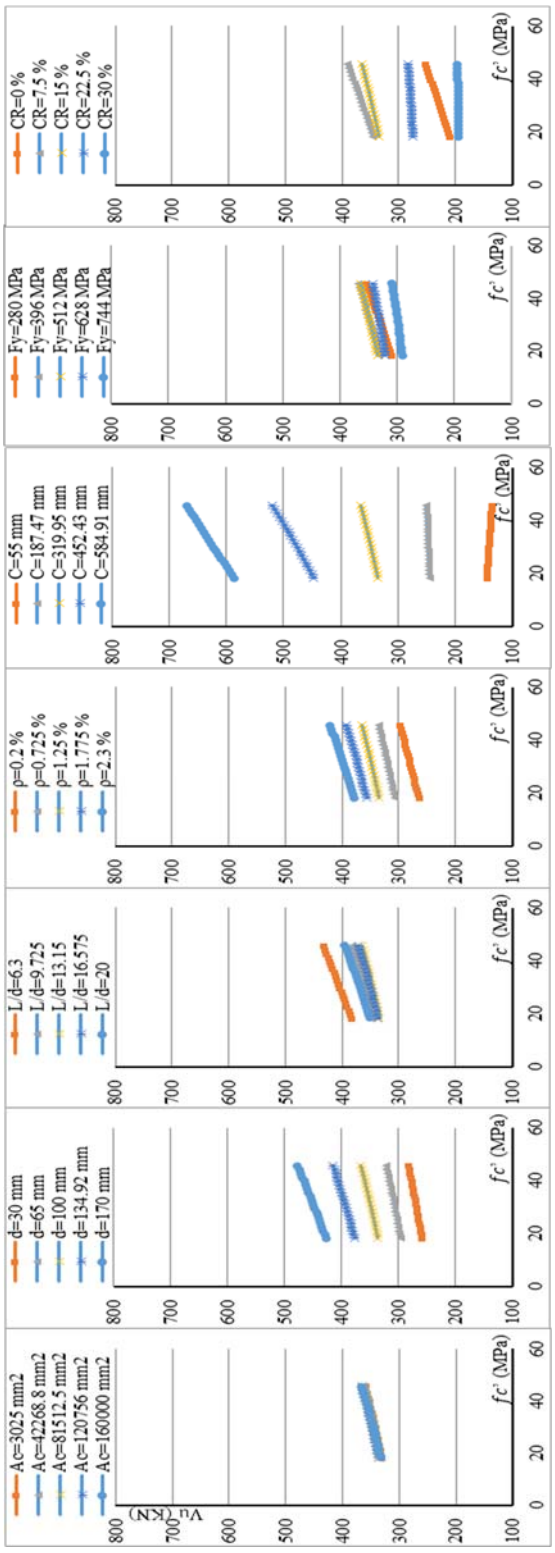

Fig. 14 Interaction effects between concrete compressive strength and other input variables.

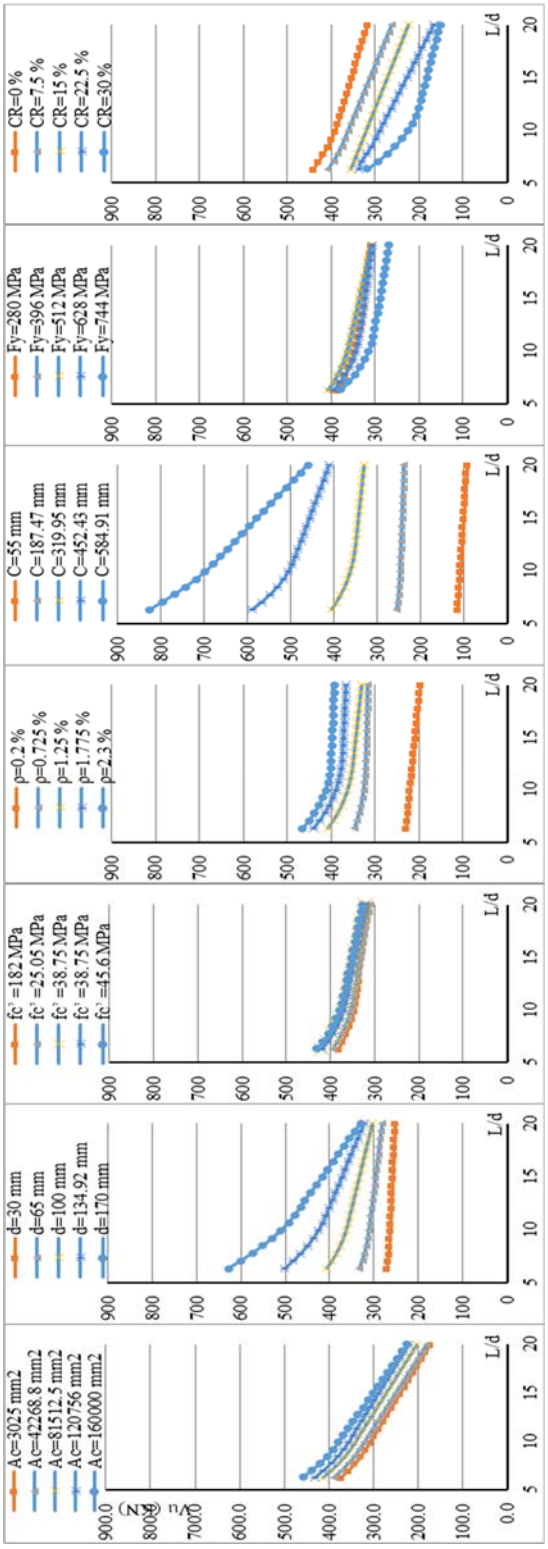

Fig. 15 Interaction effects between span-to-depth ratio and other input variables.

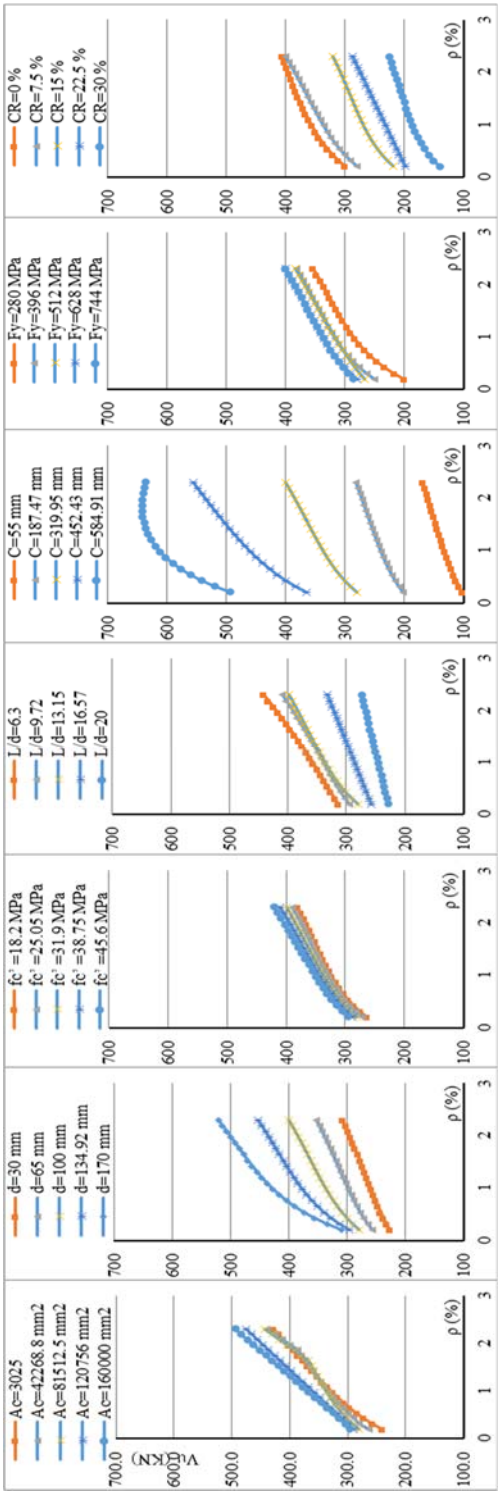

Fig. 16 Interaction effects between flexure reinforcement ratio and other input variables.

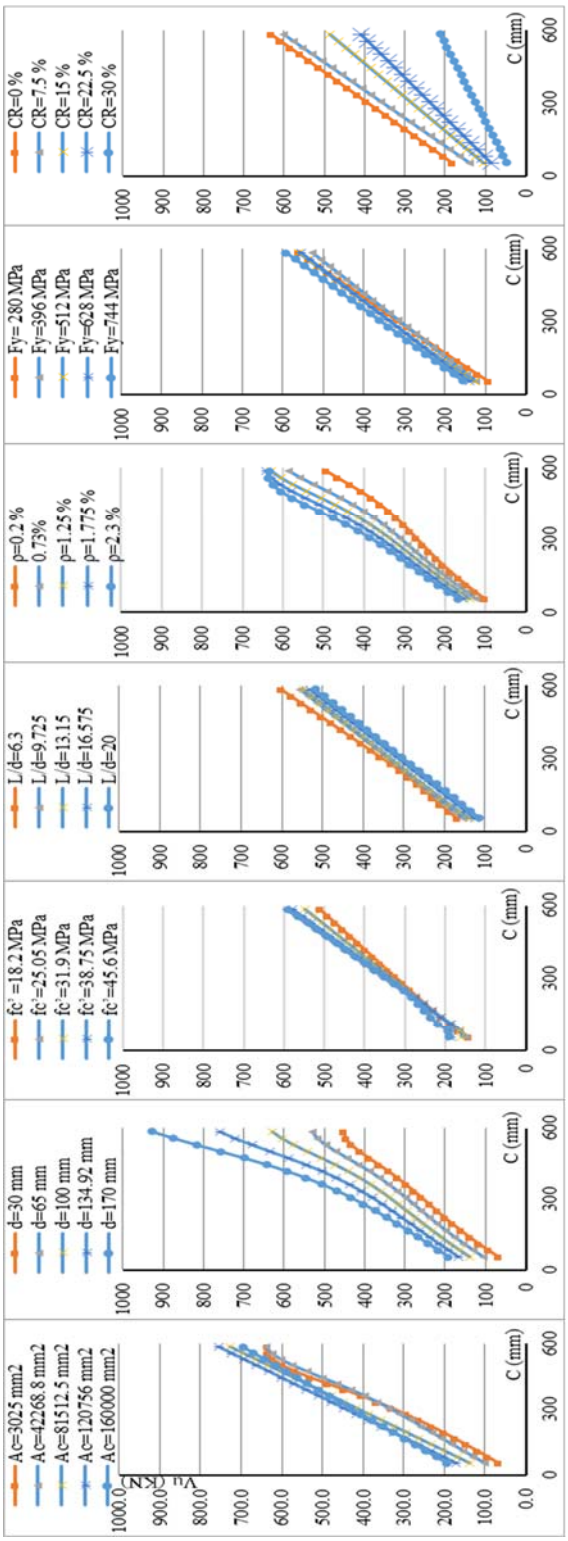

Fig. 17 Interaction effects between column width and other input variables.

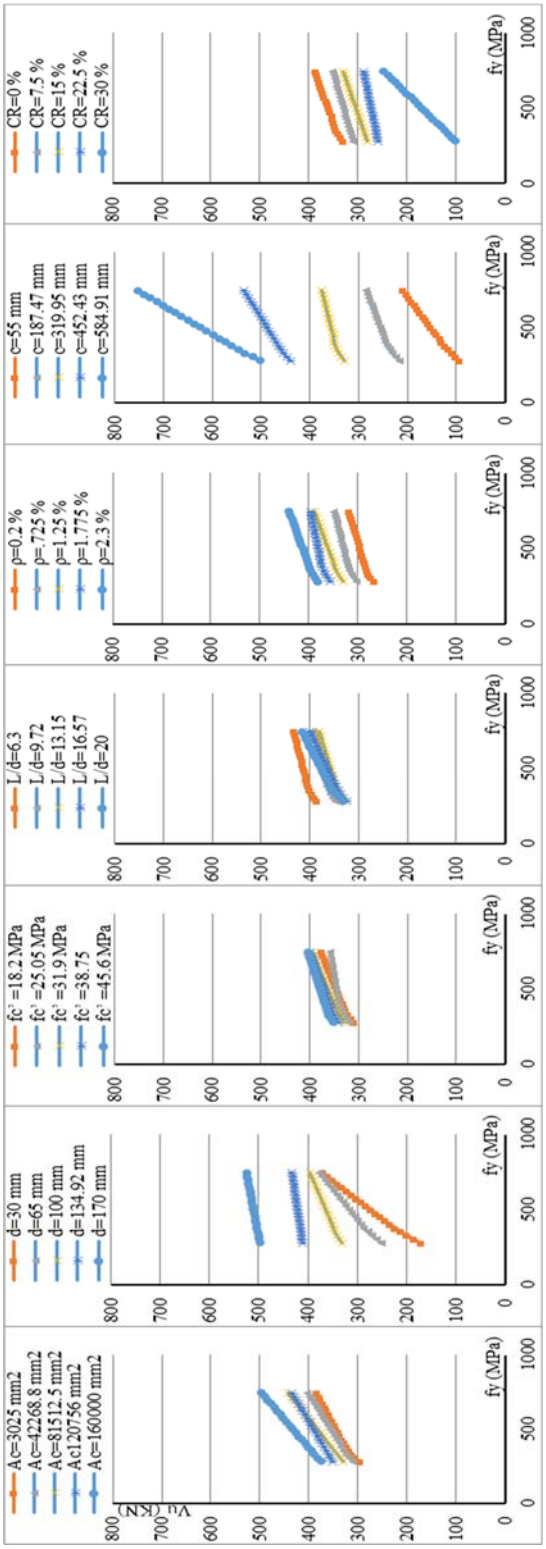

Fig. 18 Interaction effects between yield strength of reinforcement and other input variables.

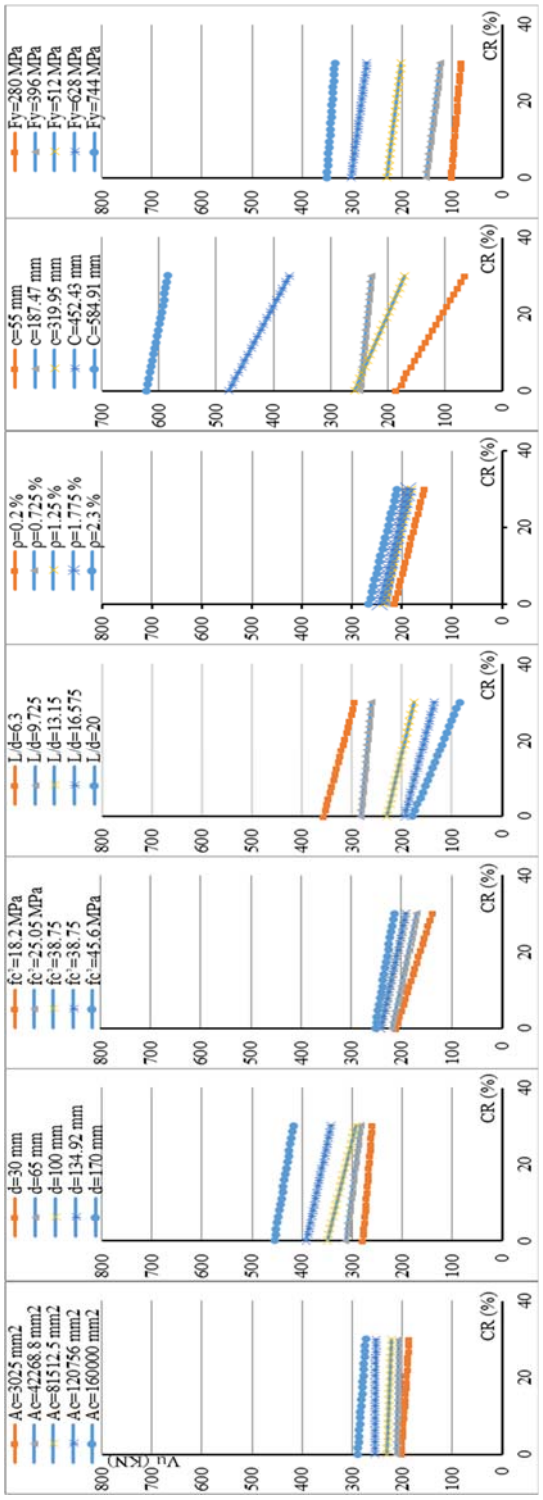

Fig. 19 Interaction effects between corrosion level and other input variables.

- Effect of reinforcement yield strength

Fig. 18 shows the ANN model predictions for the PS capacity as the reinforcement yield strength (fy) increases. The results describe that the PS capacity marginally increased as the yield strength increased. But when combined with increasing the column width, the PS capacity significantly improved. In addition, combining the increase of (d) with the increase of (fy) has a significant influence on the PS. For small values of (d), increasing the (fy) enhances the PS capacity at a higher rate.

- Effect of corrosion ratio

The sensitivity of the PS capacity to corrosion ratio (CR) combined with other parameters is represented in Fig. 19. As can be seen from the figure, the PS capacity generally decreases as (CR) increases. This is owing to the formation of cracks caused by the internal pressure resulting from the corrosion products, in addition to the mass loss of reinforcement and the bond loss between corroded rebars and concrete. Degradation in the PS capacity of corroded RC slab-column joints is proportional to corrosion level. Furthermore, the ANN model predicted higher degradation in PS capacity when increasing (CR) combined with decreasing d, decreasing (C), or increasing (L/d).

3. Conclusions

In the present study, the ANN approach was proposed to model the punching shear behavior of RC slab-column joints exposed to rebar corrosion. A total of 232 datasets extracted from experimental results in the literature along with 397 datasets obtained by numerical analysis were used to develop the proposed ANN model. Column-section area, effective slab depth, concrete compressive strength, span-to-depth ratio, reinforcement ratio, column width, reinforcement yield strength, and corrosion ratio were considered as input variables to the ANN. However, PS capacity and ultimate deflection were considered as output variables. The following is a summary of the study's key conclusions:

1. The performance of the training, testing, and validating processes of the ANN was measured by the mean squared errors, the performance implied a successful overall training process.
2. The regression model that displays the correlation between the real values and the ANN predicted values returned a coefficient of determination (R^2) equals 0.9830, 0.9871, 0.9825, and 0.984 for training, testing, validating, and all data, respectively. Thus, the developed ANN model is capable of well predicting the PS behavior of corroded and uncorroded RC SCJs.
3. A user-friendly GUI was created to predict the PS capacity and ultimate deflection of reinforced concrete slabs. This tool offers the benefit of being simpler to use compared to traditional methods such as experimental studies and finite element modeling.
4. The proposed ANN model was compared with two empirical models from the literature ((Qian et al., 2022a) and (Gomaa et al., 2023)) that predict the PS capacity of corroded RC SCJs. The mean and coefficient of variation for the ratios between experimental data and predictions are used for comparison. The returned mean and coefficient of variation values were 0.99 and 0.06 for the ANN model, 0.98 and 0.06 for [31], and

1.04 and 0.12 for [27], respectively. The proposed ANN model provided better prediction compared to other models.

5. The proposed ANN model was compared with two design codes ((ACI 318-19)[37] and (CSA 23.3–14)), the mean and coefficient of variation values were 0.89 and 0.26 for (ACI 318-19), and 0.91 and 0.26 for (CSA 23.3–14)[36], respectively. The PS capacity predicted by the available code's equations is much higher than the experimental values of the corroded RC SCJ, this is obviously because the available equations in the codes do not take corrosion into account. In contrast, the proposed ANN accurately predicts the PS behavior of the tested slabs.
6. A parametric study was performed to examine the effect of each input variable and the interaction effect between these variables on the outputs of corroded RC slabs.
7. Five thousand six hundred5600 datasets were obtained using the proposed ANN model to carry out this parametric study, it is worth highlighting that this huge number of datasets is a very hard task to achieve using conventional approaches such as experimental tests and finite element modeling.
8. The results indicated that when (L/d) increased by 52% relative to its mean value, the PS capacity was at 69% of its value at the mean (L/d), this is due to the size effect. When (C) increased by 83% relative to its mean value, the PS capacity enhanced by 75%, this is due to the reduction of stress concentration around the shorter side of the column. Increasing (fy) by 45% enhanced the PS capacity by only 2%, this insensitivity to reinforcement improving could be due to the loss of integrity between concrete and corroded rebars.
9. The parametric study revealed that column width, span-to-depth ration, effective depth, and corrosion ratio interacted significantly with one another and with other factors, indicating the strong influence of those parameters on the PS behavior compared to the other parameters.

4. Appendix (1)

No	Ac	d	fc'	L/d	ρ	C	fy	CR	Du	Vu (KN)
1	40000	118	36	14.67	0.91	200	532	0.00	Def	376
2	40000	118	39	14.67	0.91	200	435	10.00	15.00	335
3	40000	118	41	14.67	0.91	200	412	20.00	22.00	302
4	40000	118	41	14.67	0.91	200	399	30.00	23.00	289
5	40000	118	44	14.67	0.52	200	532	0.00	33.00	280
6	40000	118	44	14.67	0.52	200	471	10.00	27.00	244
7	40000	118	46	14.67	0.52	200	448	20.00	25.00	212
8	40000	118	41	14.67	0.52	200	396	30.00	14.00	192
9	40000	93	38	17.60	1.16	200	532	0.00	14.00	274
10	40000	93	41	17.60	1.16	200	423	10.00	16.00	238
11	40000	93	41	17.60	1.16	200	401	20.00	18.00	228
12	40000	93	42	17.60	1.16	200	380	30.00	21.00	215
13	40000	93	44	14.67	0.52	200	532	0.00	14.00	270
14	40000	93	44	14.67	0.52	200	471	10.00	15.50	250
15	40000	118	44	14.67	0.52	200	532	0.00	12.00	365
16	40000	118	44	14.67	0.52	200	471	10.00	13.50	340
17	40000	143	44	14.67	0.52	200	532	0.00	8.00	480
18	40000	143	44	14.67	0.52	200	471	10.00	10.00	455
19	40000	118	44	14.67	0.74	200	532	0.00	9.00	330
20	40000	118	44	14.67	0.74	200	471	10.00	11.50	310

21	40000	118	44	14.67	1.18	200	532	0.00	12.00	412
22	40000	118	44	14.67	1.18	200	471	10.00	12.50	395
23	40000	118	44	14.67	1.52	200	532	0.00	10.00	480
24	40000	118	44	14.67	1.52	200	471	10.00	11.50	433
25	62500	104	40	18.26	1.00	250	532	0.00	16.00	370
26	62500	104	40	18.26	1.00	250	471	26.00	34.00	297
27	62500	138	21	14.49	2.20	250	530	0.00	8.80	374
28	10000	80	30	12.50	0.34	100	530	0.00	11.83	115
29	10000	80	20	12.50	0.34	100	530	0.00	7.75	109
30	10000	55	32	11.45	0.34	100	533	0.00	11.00	49
31	10000	55	36	11.45	0.73	100	545	0.00	10.00	61
32	10000	75	36	8.40	0.34	100	540	0.00	9.00	79
33	10000	75	29	8.40	0.73	100	565	0.00	8.00	122
34	22500	70	26	17.40	1.00	150	530	0.00	14.40	160
35	62500	120	33	16.60	0.97	250	520	0.00	3.20	31
36	4000	120	29	16.60	1.00	63	740	0.00	6.00	272
37	100000	120	22	18.33	1.00	316	744	0.00	6.50	281
38	160000	120	26	20.00	1.00	400	740	0.00	8.00	328
39	6400	85	30	10.00	0.43	80	510	0.00	6.20	160
40	22500	120	35	8.46	0.97	150	385	0.00	10.00	223
41	22500	90	30	11.00	0.97	150	385	0.00	16.00	150
42	3600	45	30	11.60	0.20	60	280	0.00	15.76	56
43	3600	45	30	11.60	0.60	60	280	0.00	46.20	77
44	3600	45	30	11.60	1.40	60	280	0.00	27.70	99
45	3600	45	30	11.60	2.30	60	280	0.00	10.92	113
46	3600	45	30	8.33	1.40	60	280	0.00	13.16	117
47	62500	130	33	14.28	1.07	250	385	0.00	24.20	309
48	16900	102	37	12.00	0.46	130	601	0.00	11.00	224
49	40000	90	44	15.00	1.00	200	455	0.00	12.50	253
50	14400	40	32	18.30	0.25	120	556	0.00	18.00	38
51	10000	80	44	12.00	0.71	100	510	0.00	6.00	158
52	62500	105	27	8.40	0.59	250	492	0.00	3.50	284
53	10000	80	40	12.00	0.85	100	570	0.00	6.50	166
54	16900	102	37	12.00	1.40	130	601	0.00	8.00	295
55	16900	97	40	12.00	0.80	130	625	0.00	12.50	272
56	22500	92	42	11.42	1.84	150	420	0.00	7.00	241
57	40000	129	39	14.66	0.56	200	520	0.00	8.00	256
58	40000	129	39	14.66	0.87	200	520	0.00	12.00	315
59	40000	129	39	14.66	1.18	200	520	0.00	13.50	395
60	22500	110	44	12.00	1.20	150	455	0.00	11.90	253
61	40000	90	33	8.00	1.26	200	570	0.00	17.50	122
62	22500	80	18	10.00	1.20	150	385	0.00	15.99	114
63	22500	80	28	10.00	1.20	150	385	0.00	20.93	137
64	22500	80	18	10.00	0.60	150	385	0.00	7.52	146
65	22500	80	28	10.00	0.60	150	385	0.00	9.11	176
66	40000	130	29	13.30	1.00	200	410	0.00	16.40	421
67	10000	90	29	12.00	0.23	100	375	0.00	5.00	31
68	3025	30	43	10.00	1.20	55	400	0.00	5.52	51
69	3025	40	39	8.33	1.20	55	400	0.00	6.15	61
70	3025	60	39	6.25	1.20	55	400	0.00	3.96	136
71	16900	96	43	7.14	1.50	130	560	0.00	1.62	394
72	16900	96	45	7.14	1.50	130	560	0.00	1.58	361
73	16900	96	43	7.14	1.50	130	560	0.00	1.63	385
74	62500	150	27	5.00	0.86	250	459	0.00	2.11	678
75	62500	150	27	5.00	1.28	250	459	0.00	1.18	692
76	62500	150	26	7.00	0.86	250	459	0.00	3.82	443
77	62500	150	23	7.00	1.28	250	459	0.00	2.91	570
78	62500	150	25	5.00	0.86	250	459	0.00	2.17	518
79	62500	150	26	5.00	1.28	250	459	0.00	1.20	612
80	62500	150	24	7.00	0.86	250	459	0.00	3.85	535
81	62500	150	22	7.00	1.28	250	459	0.00	2.94	556
82	62500	150	22	7.00	1.28	250	454	0.00	3.12	503

83	62500	150	24	7.00	0.86	250	454	0.00	4.03	507
84	56100	150	22	7.27	1.28	237	454	0.00	1.00	510
85	56100	150	22	7.27	0.86	237	454	0.00	0.84	517
86	40000	150	24	7.50	1.28	200	454	0.00	1.00	551
87	40000	150	23	7.50	0.86	200	454	0.00	1.00	498
88	70686	150	22	6.83	1.28	266	454	0.00	2.98	519
89	70686	150	23	6.83	0.86	266	454	0.00	3.90	467
90	93025	219	42	5.74	0.87	305	459	0.00	1.04	1030
91	93025	219	42	5.74	0.87	305	459	0.00	1.04	1030
92	90000	157	18	5.41	1.25	300	583	0.00	2.40	570
93	90000	187	19	4.55	1.24	300	583	0.00	1.00	872
94	90000	145	35	3.97	0.54	300	521	0.00	1.00	495
95	5411	210	40	6.37	0.77	74	538	0.00	1.00	530
96	21642	215	38	6.03	0.75	147	538	0.00	1.00	712
97	85530	218	44	5.57	0.74	292	538	0.00	1.00	935
98	342119	212	38	4.95	0.76	585	538	0.00	1.00	1206
99	5411	215	38	6.23	1.46	74	542	0.00	1.00	656
100	21642	213	43	6.09	1.47	147	542	0.00	1.00	871
101	85530	214	42	5.68	1.47	292	542	0.00	1.30	1091
102	342119	210	37	5.00	1.50	585	542	0.00	1.40	1476
103	67600	197	35	2.93	1.59	260	517	0.00	1.00	985
104	67600	204	34	8.09	1.54	260	517	0.00	1.00	961
105	62500	150	26	7.00	0.86	250	604	0.00	1.00	443
106	62500	150	24	7.00	1.28	250	604	0.00	1.00	570
107	62500	150	28	7.00	1.73	250	454	0.00	1.96	690
108	62500	150	42	7.00	0.86	250	604	0.00	1.00	693
109	62500	150	38	7.00	1.28	250	604	0.00	1.00	771
110	62500	150	39	7.00	1.73	250	454	0.00	1.75	800
111	62500	150	53	7.00	0.86	250	454	0.00	3.44	610
112	62500	150	54	7.00	1.28	250	454	0.00	2.46	785
113	62500	150	55	7.00	1.73	250	454	0.00	1.42	860
114	70686	150	33	6.83	0.71	266	514	0.00	2.13	490
115	70686	150	35	6.83	0.93	266	514	0.00	1.59	600
116	70686	150	34	6.83	1.71	266	514	0.00	1.00	662
117	70686	150	47	6.83	0.71	266	514	0.00	1.86	574
118	70686	150	49	6.83	0.93	266	514	0.00	1.32	649
119	70686	150	52	6.83	1.71	266	514	0.00	1.00	761
120	70686	150	63	6.83	0.71	266	514	0.00	1.53	562
121	70686	150	67	6.83	0.93	266	514	0.00	0.96	622
122	70686	150	63	6.83	1.71	266	514	0.00	1.00	752
123	50625	125	30	7.64	1.10	225	434	0.00	5.77	306
124	50625	125	30	7.64	2.20	225	434	0.00	3.28	349
125	17671	90	34	4.17	0.58	133	620	0.00	1.00	240
126	41548	90	34	3.72	0.58	204	620	0.00	1.00	265
127	17671	88	35	4.26	1.29	133	619	0.00	1.00	294
128	17671	86	35	4.36	1.79	133	589	0.00	1.00	313
129	40000	100	39	2.63	0.98	200	488	0.00	1.20	330
130	40000	150	39	2.63	0.90	200	465	0.00	1.00	583
131	40000	200	39	2.63	0.83	200	465	0.00	1.00	904
132	40000	300	39	2.63	0.76	200	468	0.00	1.00	1381
133	90000	400	39	1.84	0.76	300	433	0.00	1.00	2224
134	90000	500	39	1.48	0.76	300	433	0.00	1.00	2681
135	62500	120	37	5.92	0.87	250	430	0.00	5.10	365
136	62500	120	37	5.92	0.87	250	430	0.00	5.10	365
137	14400	107	57	9.25	1.09	120	749	0.00	1.00	240
138	14400	108	59	9.17	1.08	120	749	0.00	1.00	322
139	14400	107	59	9.25	1.09	120	749	0.00	1.00	318
140	28800	109	58	8.53	1.07	170	749	0.00	1.00	246
141	28800	106	58	8.77	1.10	170	749	0.00	1.00	361
142	28800	107	57	8.69	1.09	170	749	0.00	1.00	331
143	43200	108	56	8.06	1.08	208	749	0.00	1.00	241
144	43200	107	60	8.13	1.09	208	749	0.00	1.00	400

145	43200	106	54	8.21	1.10	208	749	0.00	1.00	358
146	57600	108	56	7.50	1.08	240	749	0.00	1.00	251
147	57600	106	54	7.64	1.10	240	749	0.00	1.00	395
148	57600	107	56	7.57	1.09	240	749	0.00	1.00	404
149	72000	108	57	6.94	1.08	268	749	0.00	1.00	287
150	72000	108	67	6.94	1.08	268	749	0.00	1.00	426
151	72000	109	63	6.88	1.07	268	749	0.00	1.00	446
152	24053	172	41	1.12	1.25	155	500	0.00	1.00	789
153	24053	172	36	1.82	1.25	155	500	0.00	1.00	668
154	49087	246	33	1.12	1.18	222	500	0.00	1.00	1356
155	62500	124	36	7.06	1.51	250	488	0.00	1.00	483
156	90000	190	35	7.11	1.24	300	531	0.00	1.00	825
157	122500	260	31	6.63	1.10	350	524	0.00	1.00	1046
158	67600	210	28	5.95	1.50	260	573	0.00	1.00	1024
159	67600	210	41	5.95	0.25	260	552	0.00	1.00	439
160	270400	456	32	5.09	0.33	520	520	0.00	1.00	2153
161	67600	210	32	5.95	0.25	260	541	0.00	1.00	408
162	67600	210	29	5.95	0.33	260	555	0.00	1.00	550
163	16900	96	29	6.51	1.50	130	526	0.00	2.45	236
164	16900	100	35	6.25	0.75	130	550	0.00	2.86	243
165	16900	117	35	5.34	0.33	130	525	0.00	2.99	141
166	16900	117	29	5.34	0.25	130	525	0.00	3.28	118
167	67600	210	29	5.95	0.33	260	577	0.00	1.00	540
168	40000	100	22	5.00	0.73	200	507	0.00	3.50	188
169	40000	100	20	5.00	1.09	200	507	0.00	2.72	202
170	40000	100	74	5.00	1.50	200	471	0.00	1.86	331
171	40000	100	75	5.00	1.50	200	471	0.00	1.84	371
172	40000	100	64	5.00	2.25	200	471	0.00	0.37	405
173	40000	100	75	5.00	2.25	200	471	0.00	0.15	489
174	62500	90	26	6.94	1.06	250	454	0.00	6.50	230
175	62500	90	27	6.94	2.00	250	466	0.00	3.96	317
176	62500	130	26	4.81	0.98	250	486	0.00	1.87	443
177	40000	168	35	5.36	0.50	200	490	0.00	1.17	587
178	40000	164	34	5.49	1.30	200	507	0.00	1.00	805
179	40000	168	32	5.36	0.50	200	490	0.00	1.22	522
180	40000	164	31	5.49	1.30	200	507	0.00	1.00	797
181	164836	126	31	5.25	0.50	406	421	0.00	5.54	311
182	164836	126	28	5.25	1.00	406	421	0.00	4.47	401
183	62500	98	27	4.85	1.57	250	458	0.00	3.03	356
184	62500	128	28	3.71	1.20	250	458	0.00	1.39	470
185	62500	158	29	3.01	0.97	250	458	0.00	1.00	646
186	122500	88	23	4.83	1.75	350	458	0.00	3.23	408
187	62500	98	26	4.85	1.57	250	458	0.00	3.04	360
188	62500	99	33	4.80	1.14	250	371	0.00	6.56	357
189	62500	100	35	4.75	0.79	250	414	0.00	5.86	293
190	62500	98	41	4.85	1.57	250	458	0.00	2.75	412
191	62500	99	41	4.80	1.14	250	371	0.00	6.39	354
192	23104	165	45	4.93	0.77	152	419	0.00	2.39	600
193	23104	165	45	4.93	0.77	152	419	0.00	2.39	600
194	62500	163	33	4.86	0.52	250	435	0.00	2.79	479
195	62500	158	35	5.02	2.17	250	433	0.00	0.54	678
196	62500	163	60	4.86	0.65	250	435	0.00	1.96	675
197	62500	160	61	4.94	0.98	250	440	0.00	1.22	798
198	62500	158	61	5.02	1.13	250	433	0.00	1.29	811
199	62500	158	67	5.02	1.67	250	433	0.00	0.30	802
200	62500	138	69	5.75	2.48	250	433	0.00	0.30	788
201	62500	128	70	6.20	2.68	250	433	0.00	0.30	801
202	62500	105	34	7.52	0.40	250	450	0.00	7.68	228
203	62500	113	70	7.02	1.88	250	435	0.00	3.29	481
204	16900	193	36	6.81	1.63	130	583	0.00	1.00	682
205	67600	210	34	5.95	1.50	260	709	0.00	1.00	974
206	270400	197	37	5.69	1.59	520	583	0.00	1.00	1324

207	115600	267	31	4.53	1.58	340	550	0.00	1.00	1625
208	193600	353	32	3.29	1.50	440	580	0.00	1.00	2491
209	125664	294	33	5.44	1.20	354	577	0.00	1.00	1710
210	125664	294	33	5.44	1.20	354	577	0.00	1.00	1710
211	40000	105	36	6.33	1.00	200	523	0.00	2.96	289
212	40000	104	126	6.38	0.94	200	493	0.00	2.33	413
213	40000	102	130	6.55	1.24	200	523	0.00	0.88	429
214	40000	102	130	6.54	1.48	200	523	0.00	0.34	461
215	202500	200	37	5.13	1.07	450	575	0.00	1.00	974
216	202500	200	38	5.13	1.07	450	575	0.00	1.00	956
217	62500	150	27	5.00	0.86	250	604	0.00	1.00	678
218	62500	150	27	5.00	1.28	250	604	0.00	1.00	692
219	62500	150	37	5.00	0.86	250	604	0.00	1.00	691
220	62500	150	36	5.00	1.28	250	604	0.00	1.00	855
221	62500	150	26	7.00	0.86	250	604	0.00	1.00	443
222	62500	150	24	7.00	1.28	250	604	0.00	1.00	570
223	62500	150	42	7.00	0.86	250	604	0.00	1.00	693
224	62500	150	38	7.00	1.28	250	604	0.00	1.00	771
225	70686	155	37	6.77	2.24	266	558	0.00	1.00	612
226	70686	155	37	6.77	2.24	266	558	0.00	1.00	612
227	70686	143	51	6.29	1.48	266	540	0.00	1.00	779
228	70686	143	51	6.29	1.48	266	540	0.00	1.00	779
229	10000	60	39	7.50	1.10	100	382	0.00	10.36	120
230	10000	60	39	7.50	1.95	100	382	0.00	8.44	170
231	10000	60	39	7.50	1.95	100	382	0.00	8.44	135
232	10000	75	29	6.00	1.50	100	382	0.00	7.65	180
233	22500	170	30	7.78	0.89	150	480	0.00	2.70	180
234	22500	90	30	7.78	1.57	150	480	0.00	6.64	165
235	22500	170	30	7.78	0.89	150	480	0.00	1.00	201
236	22500	170	30	7.78	0.89	150	480	0.00	4.15	231
237	22500	90	30	7.78	0.89	150	370	15.00	14.03	131
238	22500	170	30	7.78	1.57	150	377	15.00	1.37	101
239	22500	90	30	7.78	0.89	150	468	0.00	1.68	255
240	22500	90	30	7.78	1.57	150	485	0.00	6.48	217
241	22500	90	31	7.78	1.57	150	480	5.00	7.40	195
242	22500	90	31	7.78	1.57	150	447	10.00	9.24	171
243	22500	90	30	7.78	1.57	150	385	15.00	12.01	145
244	22500	90	30	7.78	1.57	150	377	20.00	13.06	125
245	22500	90	30	7.78	1.57	150	360	25.00	14.39	120
246	22500	90	30	7.78	1.57	150	334	30.00	16.00	102
247	22500	90	30	7.78	1.57	150	385	15.00	8.57	118
248	22500	90	30	7.78	1.57	150	385	15.00	5.13	98
249	22500	130	30	7.78	1.57	150	385	15.00	10.00	142
250	22500	170	30	7.78	1.57	150	385	15.00	7.99	150
251	22500	90	30	7.78	0.89	150	385	15.00	13.55	118
252	22500	90	30	7.78	1.12	150	385	15.00	13.03	123
253	16900	96	43	7.14	1.50	130	560	2.50	2.01	366
254	16900	96	45	7.14	1.50	130	560	2.50	1.97	336
255	16900	96	43	7.14	1.50	130	560	2.50	2.02	358
256	62500	150	27	5.00	0.86	250	459	2.50	2.51	631
257	62500	150	27	5.00	1.28	250	459	2.50	1.57	644
258	62500	150	26	7.00	0.86	250	459	2.50	4.22	412
259	62500	150	23	7.00	1.28	250	459	2.50	3.31	530
260	62500	150	25	5.00	0.86	250	459	2.50	2.57	482
261	62500	150	26	5.00	1.28	250	459	2.50	1.59	569
262	62500	150	24	7.00	0.86	250	459	2.50	4.25	498
263	62500	150	22	7.00	1.28	250	459	2.50	3.33	517
264	62500	150	22	7.00	1.28	250	454	2.50	3.51	468
265	62500	150	24	7.00	0.86	250	454	2.50	4.42	472
266	56100	150	22	7.27	1.28	237	454	2.50	0.29	474
267	56100	150	22	7.27	0.86	237	454	2.50	1.23	481
268	40000	150	24	7.50	1.28	200	454	2.50	1.00	512

269	40000	150	23	7.50	0.86	200	454	2.50	1.00	463
270	70686	150	22	6.83	1.28	266	454	2.50	3.38	483
271	70686	150	23	6.83	0.86	266	454	2.50	4.30	434
272	93025	219	42	5.74	0.87	305	459	2.50	1.00	958
273	93025	219	42	5.74	0.87	305	459	2.50	1.00	958
274	90000	157	18	5.41	1.25	300	583	7.50	1.00	502
275	90000	187	19	4.55	1.24	300	583	7.50	1.00	767
276	90000	145	35	3.97	0.54	300	521	7.50	1.00	436
277	5411	210	40	6.37	0.77	74	538	7.50	1.00	466
278	21642	215	38	6.03	0.75	147	538	7.50	1.00	627
279	85530	218	44	5.57	0.74	292	538	7.50	1.00	823
280	342119	212	38	4.95	0.76	585	538	5.00	1.00	1061
281	5411	215	38	6.23	1.46	74	542	5.00	1.00	577
282	21642	213	43	6.09	1.47	147	542	5.00	1.00	766
283	85530	214	42	5.68	1.47	292	542	5.00	1.00	960
284	342119	210	37	5.00	1.50	585	542	5.00	1.00	1299
285	67600	197	35	2.93	1.59	260	517	5.00	1.00	867
286	67600	204	34	8.09	1.54	260	517	5.00	1.00	846
287	62500	150	26	7.00	0.86	250	604	7.50	1.00	390
288	62500	150	24	7.00	1.28	250	604	7.50	1.00	502
289	62500	150	28	7.00	1.73	250	454	7.50	3.15	607
290	62500	150	42	7.00	0.86	250	604	7.50	0.08	610
291	62500	150	38	7.00	1.28	250	604	7.50	1.00	678
292	62500	150	39	7.00	1.73	250	454	7.50	2.94	704
293	62500	150	53	7.00	0.86	250	454	7.50	4.62	537
294	62500	150	54	7.00	1.28	250	454	7.50	3.64	691
295	62500	150	55	7.00	1.73	250	454	7.50	2.60	757
296	70686	150	33	6.83	0.71	266	514	7.50	3.31	431
297	70686	150	35	6.83	0.93	266	514	7.50	2.77	528
298	70686	150	34	6.83	1.71	266	514	7.50	1.03	582
299	70686	150	47	6.83	0.71	266	514	7.50	3.05	505
300	70686	150	49	6.83	0.93	266	514	7.50	2.50	571
301	70686	150	52	6.83	1.71	266	514	7.50	0.67	670
302	70686	150	63	6.83	0.71	266	514	7.50	2.72	495
303	70686	150	67	6.83	0.93	266	514	7.50	2.14	548
304	70686	150	63	6.83	1.71	266	514	7.50	0.46	662
305	16900	96	43	7.14	1.50	130	560	12.50	3.59	299
306	16900	96	45	7.14	1.50	130	560	12.50	3.55	275
307	16900	96	43	7.14	1.50	130	560	15.00	4.00	293
308	62500	150	27	5.00	0.86	250	459	15.00	4.48	515
309	62500	150	27	5.00	1.28	250	459	15.00	3.55	526
310	62500	150	26	7.00	0.86	250	459	15.00	6.19	337
311	62500	150	23	7.00	1.28	250	459	15.00	5.28	433
312	62500	150	25	5.00	0.86	250	459	15.00	4.54	394
313	62500	150	26	5.00	1.28	250	459	15.00	3.57	465
314	62500	150	24	7.00	0.86	250	459	12.50	5.83	407
315	62500	150	22	7.00	1.28	250	459	12.50	4.91	423
316	62500	150	22	7.00	1.28	250	454	12.50	5.09	383
317	62500	150	24	7.00	0.86	250	454	12.50	6.00	385
318	56100	150	22	7.27	1.28	237	454	12.50	1.87	388
319	56100	150	22	7.27	0.86	237	454	12.50	2.81	393
320	40000	150	24	7.50	1.28	200	454	12.50	1.00	419
321	40000	150	23	7.50	0.86	200	454	12.50	1.00	379
322	70686	150	22	6.83	1.28	266	454	12.50	4.96	394
323	70686	150	23	6.83	0.86	266	454	12.50	5.88	355
324	93025	219	42	5.74	0.87	305	459	12.50	0.94	783
325	93025	219	42	5.74	0.87	305	459	12.50	0.94	783
326	90000	157	18	5.41	1.25	300	583	12.50	1.00	433
327	90000	187	19	4.55	1.24	300	583	12.50	1.00	663
328	90000	145	35	3.97	0.54	300	521	12.50	2.10	376
329	5411	210	40	6.37	0.77	74	538	12.50	1.00	403
330	21642	215	38	6.03	0.75	147	538	12.50	1.00	541

331	85530	218	44	5.57	0.74	292	538	12.50	1.00	711
332	342119	212	38	4.95	0.76	585	538	12.50	1.00	917
333	5411	215	38	6.23	1.46	74	542	12.50	1.00	499
334	21642	213	43	6.09	1.47	147	542	12.50	1.00	662
335	85530	214	42	5.68	1.47	292	542	12.50	1.00	829
336	342119	210	37	5.00	1.50	585	542	12.50	1.00	1122
337	67600	197	35	2.93	1.59	260	517	20.00	1.00	749
338	67600	204	34	8.09	1.54	260	517	20.00	1.63	730
339	62500	150	26	7.00	0.86	250	604	20.00	2.39	337
340	62500	150	24	7.00	1.28	250	604	20.00	1.48	376
341	62500	150	28	7.00	1.73	250	454	20.00	5.12	455
342	62500	150	42	7.00	0.86	250	604	20.00	2.06	457
343	62500	150	38	7.00	1.28	250	604	20.00	1.18	509
344	62500	150	39	7.00	1.73	250	454	20.00	4.91	528
345	62500	150	53	7.00	0.86	250	454	17.50	6.20	403
346	62500	150	54	7.00	1.28	250	454	17.50	5.22	518
347	62500	150	55	7.00	1.73	250	454	17.50	4.18	568
348	70686	150	33	6.83	0.71	266	514	17.50	4.89	323
349	70686	150	35	6.83	0.93	266	514	17.50	4.35	396
350	70686	150	34	6.83	1.71	266	514	17.50	2.61	437
351	70686	150	47	6.83	0.71	266	514	17.50	4.63	379
352	70686	150	49	6.83	0.93	266	514	17.50	4.08	429
353	70686	150	52	6.83	1.71	266	514	17.50	2.25	503
354	70686	150	63	6.83	0.71	266	514	17.50	4.30	371
355	70686	150	67	6.83	0.93	266	514	17.50	3.72	411
356	70686	150	63	6.83	1.71	266	514	17.50	2.04	496
357	16900	96	43	7.14	1.50	130	560	17.50	4.38	260
358	16900	96	45	7.14	1.50	130	560	17.50	4.34	238
359	16900	96	43	7.14	1.50	130	560	17.50	4.39	254
360	62500	150	27	5.00	0.86	250	459	17.50	4.88	447
361	62500	150	27	5.00	1.28	250	459	17.50	3.94	457
362	62500	150	26	7.00	0.86	250	459	17.50	6.59	292
363	62500	150	23	7.00	1.28	250	459	17.50	5.68	376
364	62500	150	25	5.00	0.86	250	459	17.50	4.94	342
365	62500	150	26	5.00	1.28	250	459	17.50	3.96	404
366	62500	150	24	7.00	0.86	250	459	17.50	6.62	353
367	62500	150	22	7.00	1.28	250	459	17.50	5.70	367
368	62500	150	22	7.00	1.28	250	454	17.50	5.88	332
369	62500	150	24	7.00	0.86	250	454	17.50	6.79	335
370	56100	150	22	7.27	1.28	237	454	17.50	2.66	337
371	56100	150	22	7.27	0.86	237	454	17.50	3.60	341
372	40000	150	24	7.50	1.28	200	454	17.50	1.09	364
373	40000	150	23	7.50	0.86	200	454	22.50	2.31	309
374	70686	150	22	6.83	1.28	266	454	22.50	6.54	322
375	70686	150	23	6.83	0.86	266	454	22.50	7.46	290
376	93025	219	42	5.74	0.87	305	459	22.50	2.52	639
377	93025	219	42	5.74	0.87	305	459	22.50	2.52	639
378	90000	157	18	5.41	1.25	300	583	22.50	1.07	353
379	90000	187	19	4.55	1.24	300	583	22.50	1.10	541
380	90000	145	35	3.97	0.54	300	521	22.50	3.68	307
381	5411	210	40	6.37	0.77	74	538	22.50	1.20	329
382	21642	215	38	6.03	0.75	147	538	22.50	0.78	441
383	85530	218	44	5.57	0.74	292	538	22.50	0.18	580
384	342119	212	38	4.95	0.76	585	538	22.50	0.22	748
385	5411	215	38	6.23	1.46	74	542	25.00	1.00	407
386	21642	213	43	6.09	1.47	147	542	25.00	1.00	540
387	85530	214	42	5.68	1.47	292	542	25.00	1.00	676
388	342119	210	37	5.00	1.50	585	542	25.00	1.00	915
389	67600	197	35	2.93	1.59	260	517	25.00	1.00	611
390	67600	204	34	8.09	1.54	260	517	25.00	2.42	596
391	62500	150	26	7.00	0.86	250	604	25.00	3.18	275
392	62500	150	24	7.00	1.28	250	604	25.00	2.27	353

393	62500	150	28	7.00	1.73	250	454	25.00	5.91	428
394	62500	150	42	7.00	0.86	250	604	25.00	2.85	430
395	62500	150	38	7.00	1.28	250	604	22.50	1.57	478
396	62500	150	39	7.00	1.73	250	454	22.50	5.31	496
397	62500	150	53	7.00	0.86	250	454	22.50	6.99	378
398	62500	150	54	7.00	1.28	250	454	22.50	6.01	487
399	62500	150	55	7.00	1.73	250	454	22.50	4.97	533
400	70686	150	33	6.83	0.71	266	514	22.50	5.68	304
401	70686	150	35	6.83	0.93	266	514	22.50	5.14	372
402	70686	150	34	6.83	1.71	266	514	22.50	3.40	410
403	70686	150	47	6.83	0.71	266	514	22.50	5.42	356
404	70686	150	49	6.83	0.93	266	514	22.50	4.87	403
405	70686	150	52	6.83	1.71	266	514	22.50	3.04	472
406	70686	150	63	6.83	0.71	266	514	22.50	5.09	348
407	70686	150	67	6.83	0.93	266	514	22.50	4.51	386
408	70686	150	63	6.83	1.71	266	514	22.50	2.83	466
409	50625	125	30	7.64	1.10	225	434	22.50	9.32	190
410	50625	125	30	7.64	2.20	225	434	22.50	6.84	216
411	17671	90	34	4.17	0.58	133	620	22.50	3.37	149
412	41548	90	34	3.72	0.58	204	620	22.50	3.02	164
413	17671	88	35	4.26	1.29	133	619	22.50	1.95	350
414	17671	86	35	4.36	1.79	133	589	22.50	1.95	542
415	40000	100	39	2.63	0.98	200	488	22.50	4.76	829
416	40000	150	39	2.63	0.90	200	465	27.50	3.95	1334
417	40000	200	39	2.63	0.83	200	465	27.50	1.59	1609
418	40000	300	39	2.63	0.76	200	468	27.50	1.00	219
419	90000	400	39	1.84	0.76	300	433	27.50	1.00	219
420	90000	500	39	1.48	0.76	300	433	27.50	1.00	144
421	62500	120	37	5.92	0.87	250	430	27.50	9.44	193
422	62500	120	37	5.92	0.87	250	430	27.50	9.44	191
423	14400	107	57	9.25	1.09	120	749	27.50	1.83	148
424	14400	108	59	9.17	1.08	120	749	27.50	1.69	217
425	14400	107	59	9.25	1.09	120	749	27.50	1.79	199
426	28800	109	58	8.53	1.07	170	749	27.50	1.00	145
427	28800	106	58	8.77	1.10	170	749	27.50	1.00	240
428	28800	107	57	8.69	1.09	170	749	27.50	1.00	215
429	43200	108	56	8.06	1.08	208	749	27.50	1.00	151
430	43200	107	60	8.13	1.09	208	749	27.50	1.00	237
431	43200	106	54	8.21	1.10	208	749	27.50	1.00	242
432	57600	108	56	7.50	1.08	240	749	27.50	1.00	172
433	57600	106	54	7.64	1.10	240	749	27.50	1.00	256
434	57600	107	56	7.57	1.09	240	749	27.50	1.00	268
435	72000	108	57	6.94	1.08	268	749	27.50	1.00	473
436	72000	108	67	6.94	1.08	268	749	27.50	1.00	401
437	72000	109	63	6.88	1.07	268	749	27.50	1.00	814
438	24053	172	41	1.12	1.25	155	500	27.50	1.00	290
439	24053	172	36	1.82	1.25	155	500	27.50	0.32	495
440	49087	246	33	1.12	1.18	222	500	27.50	1.00	628
441	62500	124	36	7.06	1.51	250	488	27.50	6.92	614
442	90000	190	35	7.11	1.24	300	531	27.50	2.93	263
443	122500	260	31	6.63	1.10	350	524	27.50	0.35	1292
444	67600	210	28	5.95	1.50	260	573	27.50	0.83	245
445	67600	210	41	5.95	0.25	260	552	27.50	2.41	330
446	270400	456	32	5.09	0.33	520	520	27.50	9.55	142
447	67600	210	32	5.95	0.25	260	541	27.50	2.92	146
448	67600	210	29	5.95	0.33	260	555	27.50	2.36	85
449	16900	96	29	6.51	1.50	130	526	27.50	6.80	71
450	16900	100	35	6.25	0.75	130	550	27.50	7.21	324
451	16900	117	35	5.34	0.33	130	525	27.50	7.33	113
452	16900	117	29	5.34	0.25	130	525	27.50	7.62	121
453	67600	210	29	5.95	0.33	260	577	27.50	1.68	199
454	40000	100	22	5.00	0.73	200	507	27.50	7.85	223

455	40000	100	20	5.00	1.09	200	507	27.50	7.07	243
456	40000	100	74	5.00	1.50	200	471	27.50	6.20	293
457	40000	100	75	5.00	1.50	200	471	27.50	6.18	138
458	40000	100	64	5.00	2.25	200	471	27.50	4.71	190
459	40000	100	75	5.00	2.25	200	471	27.50	4.49	266
460	62500	90	26	6.94	1.06	250	454	27.50	10.84	352
461	62500	90	27	6.94	2.00	250	466	27.50	8.30	483
462	62500	130	26	4.81	0.98	250	486	27.50	6.22	313
463	40000	168	35	5.36	0.50	200	490	27.50	5.52	478
464	40000	164	34	5.49	1.30	200	507	27.50	3.49	187
465	40000	168	32	5.36	0.50	200	490	27.50	5.57	241
466	40000	164	31	5.49	1.30	200	507	27.50	3.56	214
467	164836	126	31	5.25	0.50	406	421	27.50	9.88	282
468	164836	126	28	5.25	1.00	406	421	27.50	8.82	388
469	62500	98	27	4.85	1.57	250	458	27.50	7.37	245
470	62500	128	28	3.71	1.20	250	458	27.50	5.74	216
471	62500	158	29	3.01	0.97	250	458	27.50	4.13	214
472	122500	88	23	4.83	1.75	350	458	27.50	7.57	176
473	62500	98	26	4.85	1.57	250	458	27.50	7.39	247
474	62500	99	33	4.80	1.14	250	371	27.50	10.90	212
475	62500	100	35	4.75	0.79	250	414	27.50	10.21	360
476	62500	98	41	4.85	1.57	250	458	27.50	7.10	360
477	62500	99	41	4.80	1.14	250	371	27.50	10.74	287
478	23104	165	45	4.93	0.77	152	419	27.50	6.74	407
479	23104	165	45	4.93	0.77	152	419	27.50	6.74	405
480	62500	163	33	4.86	0.52	250	435	27.50	7.13	479
481	62500	158	35	5.02	2.17	250	433	27.50	3.81	487
482	62500	163	60	4.86	0.65	250	435	27.50	6.30	481
483	62500	160	61	4.94	0.98	250	440	27.50	5.57	473
484	62500	158	61	5.02	1.13	250	433	27.50	5.64	481
485	62500	158	67	5.02	1.67	250	433	27.50	4.30	137
486	62500	138	69	5.75	2.48	250	433	27.50	4.04	289
487	62500	128	70	6.20	2.68	250	433	27.50	4.45	409
488	62500	105	34	7.52	0.40	250	450	27.50	12.02	584
489	62500	113	70	7.02	1.88	250	435	27.50	7.64	794
490	16900	193	36	6.81	1.63	130	583	27.50	1.00	975
491	67600	210	34	5.95	1.50	260	709	27.50	1.00	1495
492	270400	197	37	5.69	1.59	520	583	27.50	1.00	1026
493	115600	267	31	4.53	1.58	340	550	27.50	1.00	1026
494	193600	353	32	3.29	1.50	440	580	27.50	1.00	174
495	125664	294	33	5.44	1.20	354	577	30.00	1.00	248
496	125664	294	33	5.44	1.20	354	577	30.00	1.00	257
497	40000	105	36	6.33	1.00	200	523	30.00	7.70	277
498	40000	104	126	6.38	0.94	200	493	30.00	7.07	584
499	40000	102	130	6.55	1.24	200	523	30.00	5.62	574
500	40000	102	130	6.54	1.48	200	523	30.00	5.08	407
501	202500	200	37	5.13	1.07	450	575	30.00	0.19	415
502	202500	200	38	5.13	1.07	450	575	30.00	0.19	415
503	62500	150	27	5.00	0.86	250	604	30.00	2.26	513
504	62500	150	27	5.00	1.28	250	604	30.00	1.32	266
505	62500	150	37	5.00	0.86	250	604	30.00	2.07	342
506	62500	150	36	5.00	1.28	250	604	30.00	1.14	416
507	62500	150	26	7.00	0.86	250	604	30.00	3.97	463
508	62500	150	24	7.00	1.28	250	604	30.00	3.04	367
509	62500	150	42	7.00	0.86	250	604	30.00	3.64	367
510	62500	150	38	7.00	1.28	250	604	30.00	2.76	467
511	70686	155	37	6.77	2.24	266	558	30.00	1.64	467
512	70686	155	37	6.77	2.24	266	558	30.00	1.64	612
513	70686	143	51	6.29	1.48	266	540	30.00	3.86	779
514	70686	143	51	6.29	1.48	266	540	30.00	3.86	779
515	70686	150	33	6.83	0.71	266	514	5.00	2.92	441
516	70686	150	35	6.83	0.93	266	514	5.00	2.38	540

517	70686	150	34	6.83	1.71	266	514	5.00	0.64	596
518	70686	150	47	6.83	0.71	266	514	5.00	2.65	516
519	70686	150	49	6.83	0.93	266	514	5.00	2.11	584
520	70686	150	52	6.83	1.71	266	514	5.00	0.28	685
521	70686	150	63	6.83	0.71	266	514	5.00	2.32	506
522	70686	150	67	6.83	0.93	266	514	5.00	1.75	560
523	70686	150	63	6.83	1.71	266	514	5.00	0.07	677
524	50625	125	30	7.64	1.10	225	434	5.00	6.56	275
525	50625	125	30	7.64	2.20	225	434	5.00	4.07	314
526	17671	90	34	4.17	0.58	133	620	5.00	0.61	216
527	41548	90	34	3.72	0.58	204	620	5.00	0.25	239
528	17671	88	35	4.26	1.29	133	619	5.00	1.00	265
529	17671	86	35	4.36	1.79	133	589	5.00	1.00	282
530	40000	100	39	2.63	0.98	200	488	5.00	1.99	297
531	40000	150	39	2.63	0.90	200	465	5.00	0.40	525
532	40000	200	39	2.63	0.83	200	465	5.00	1.00	814
533	40000	300	39	2.63	0.76	200	468	5.00	1.00	1243
534	90000	400	39	1.84	0.76	300	433	5.00	1.00	2002
535	90000	500	39	1.48	0.76	300	433	5.00	1.00	2413
536	62500	120	37	5.92	0.87	250	430	5.00	5.89	329
537	62500	120	37	5.92	0.87	250	430	5.00	5.89	329
538	14400	107	57	9.25	1.09	120	749	5.00	1.00	216
539	14400	108	59	9.17	1.08	120	749	5.00	1.00	290
540	14400	107	59	9.25	1.09	120	749	5.00	1.00	286
541	28800	109	58	8.53	1.07	170	749	5.00	1.00	221
542	28800	106	58	8.77	1.10	170	749	5.00	1.00	325
543	28800	107	57	8.69	1.09	170	749	10.00	1.00	314
544	43200	108	56	8.06	1.08	208	749	10.00	1.00	229
545	43200	107	60	8.13	1.09	208	749	10.00	1.00	380
546	43200	106	54	8.21	1.10	208	749	10.00	1.00	340
547	57600	108	56	7.50	1.08	240	749	10.00	1.00	238
548	57600	106	54	7.64	1.10	240	749	10.00	1.00	375
549	57600	107	56	7.57	1.09	240	749	10.00	1.00	384
550	72000	108	57	6.94	1.08	268	749	10.00	1.00	273
551	72000	108	67	6.94	1.08	268	749	10.00	1.00	405
552	72000	109	63	6.88	1.07	268	749	10.00	1.00	424
553	24053	172	41	1.12	1.25	155	500	10.00	1.00	750
554	24053	172	36	1.82	1.25	155	500	10.00	1.00	635
555	49087	246	33	1.12	1.18	222	500	10.00	1.00	1288
556	62500	124	36	7.06	1.51	250	488	10.00	4.15	459
557	90000	190	35	7.11	1.24	300	531	10.00	0.17	784
558	122500	260	31	6.63	1.10	350	524	10.00	1.00	994
559	67600	210	28	5.95	1.50	260	573	10.00	1.00	973
560	67600	210	41	5.95	0.25	260	552	10.00	1.00	417
561	270400	456	32	5.09	0.33	520	520	10.00	1.00	2045
562	67600	210	32	5.95	0.25	260	541	10.00	0.16	388
563	67600	210	29	5.95	0.33	260	555	10.00	1.00	523
564	16900	96	29	6.51	1.50	130	526	10.00	4.03	224
565	16900	100	35	6.25	0.75	130	550	10.00	4.44	231
566	16900	117	35	5.34	0.33	130	525	10.00	4.57	134
567	16900	117	29	5.34	0.25	130	525	10.00	4.86	112
568	62500	100	30	4.75	0.79	250	414	10.00	7.44	270
569	40000	100	70	5.00	2.25	200	471	10.00	1.73	460
570	67600	210	29	5.95	0.33	260	577	10.00	1.00	513
571	40000	100	22	5.00	0.73	200	507	10.00	5.08	179
572	40000	100	20	5.00	1.09	200	507	10.00	4.30	192
573	40000	100	74	5.00	1.50	200	471	10.00	3.44	314
574	40000	100	75	5.00	1.50	200	471	10.00	3.42	352
575	40000	100	64	5.00	2.25	200	471	10.00	1.95	385
576	40000	100	75	5.00	2.25	200	471	10.00	1.73	465
577	62500	90	26	6.94	1.06	250	454	10.00	8.08	219
578	40000	90	20	5.00	1.09	200	507	10.00	4.30	185

579	40000	90	74	5.00	1.50	200	471	10.00	3.44	300
580	40000	90	75	5.00	1.50	200	471	10.00	3.42	340
581	62500	90	27	6.94	2.00	250	466	10.00	5.54	301
582	62500	130	26	4.81	0.98	250	486	10.00	3.45	421
583	40000	168	35	5.36	0.50	200	490	10.00	2.75	557
584	40000	164	34	5.49	1.30	200	507	10.00	0.73	765
585	40000	168	32	5.36	0.50	200	490	10.00	2.80	496
586	40000	164	31	5.49	1.30	200	507	10.00	0.80	757
587	164836	126	31	5.25	0.50	406	421	10.00	7.12	295
588	164836	126	28	5.25	1.00	406	421	10.00	6.05	381
589	62500	98	27	4.85	1.57	250	458	10.00	4.61	338
590	62500	128	28	3.71	1.20	250	458	10.00	2.97	447
591	62500	158	29	3.01	0.97	250	458	10.00	1.37	614
592	122500	88	23	4.83	1.75	350	458	10.00	4.81	388
593	62500	98	26	4.85	1.57	250	458	10.00	4.62	342
594	62500	99	33	4.80	1.14	250	371	10.00	8.14	339
595	62500	100	35	4.75	0.79	250	414	10.00	7.44	278
596	62500	98	41	4.85	1.57	250	458	10.00	4.33	391
597	62500	99	41	4.80	1.14	250	371	10.00	7.97	336
598	23104	165	45	4.93	0.77	152	419	10.00	3.97	570
599	23104	165	45	4.93	0.77	152	419	15.00	4.76	492
600	62500	163	33	4.86	0.52	250	435	15.00	5.16	393
601	62500	158	35	5.02	2.17	250	433	15.00	1.83	556
602	62500	163	60	4.86	0.65	250	435	15.00	4.33	554
603	62500	160	61	4.94	0.98	250	440	15.00	3.59	654
604	62500	158	61	5.02	1.13	250	433	15.00	3.66	665
605	62500	158	67	5.02	1.67	250	433	15.00	2.32	658
606	62500	138	69	5.75	2.48	250	433	15.00	2.07	646
607	62500	128	70	6.20	2.68	250	433	15.00	2.47	657
608	62500	105	34	7.52	0.40	250	450	15.00	10.05	187
609	40000.00	100.00	39.40	2.63	0.98	200.00	488.00	22.50	4.76	828.60
610	40000.00	150.00	39.40	2.63	0.90	200.00	465.00	27.50	3.95	1334.40
611	40000.00	200.00	39.40	2.63	0.83	200.00	465.00	27.50	1.59	1608.60
612	40000.00	300.00	39.40	2.63	0.76	200.00	468.00	27.50	1.00	219.00
613	90000.00	400.00	39.40	1.84	0.76	300.00	433.00	27.50	1.00	219.00
614	90000.00	500.00	39.40	1.48	0.76	300.00	433.00	27.50	1.00	144.00
615	62500.00	120.00	36.80	5.92	0.87	250.00	430.00	27.50	9.44	193.20
616	62500.00	120.00	36.80	5.92	0.87	250.00	430.00	27.50	9.44	190.80
617	14400.00	107.00	57.00	9.25	1.09	120.00	749.00	27.50	1.83	147.60
618	14400.00	108.00	59.00	9.17	1.08	120.00	749.00	27.50	1.69	216.60
619	14400.00	107.00	59.00	9.25	1.09	120.00	749.00	27.50	1.79	198.60
620	28800.00	109.00	58.00	8.53	1.07	169.71	749.00	27.50	1.00	144.60
621	28800.00	106.00	58.00	8.77	1.10	169.71	749.00	27.50	1.00	240.00
622	28800.00	107.00	57.00	8.69	1.09	169.71	749.00	27.50	1.00	214.80
623	43200.00	108.00	56.00	8.06	1.08	207.85	749.00	27.50	1.00	150.60
624	43200.00	107.00	60.00	8.13	1.09	207.85	749.00	27.50	1.00	237.00
625	43200.00	106.00	54.00	8.21	1.10	207.85	749.00	27.50	1.00	242.40
626	57600.00	108.00	56.00	7.50	1.08	240.00	749.00	27.50	1.00	172.20
627	57600.00	106.00	54.00	7.64	1.10	240.00	749.00	27.50	1.00	255.60
628	57600.00	107.00	56.00	7.57	1.09	240.00	749.00	27.50	1.00	267.60
629	377	62500	113	70	7.02	1.88	250	435	15.00	394

5. References

[1] E. Yooprasertchai, Y. Tiawilai, T. Wittayawanitchai, J. Angsumalee, P. Joyklad, and Q. Hussain, "Effect of shape, number, and location of openings on punching shear capacity of flat slabs," *Buildings*, vol. 11, no. 10, 2021, doi: 10.3390/buildings11100484.

[2] M. A. L. Silva, K. V. Dedigamuwa, and J. C. P. H. Gamage, "Performance of severely damaged reinforced concrete flat slab-column connections strengthened with Carbon Fiber Reinforced Polymer," *Compos. Struct.*, vol. 255, no. August 2020, p. 112963, 2021, doi: 10.1016/j.compstruct.2020.112963.

[3] V.-L. Tran and S.-E. %J E. with C. Kim, "A practical ANN model for predicting the PSS of two-way reinforced concrete slabs," vol.

37, pp. 2303–2327, 2021.
[4] I. Faridmehr, M. L. Nehdi, and M. H. %J E. S. Baghban, "Novel informational bat-ANN model for predicting punching shear of RC flat slabs without shear reinforcement," vol. 256, p. 114030, 2022.
[5] A. M. Gomaa, M. A. Ahmed, E. M. Lotfy, and E. A. Latef, "Strengthening of corroded reinforced concrete beams exposed to torsional and flexural stresses," *Technology*, no. April 2023, 2019, [Online]. Available: https://www.researchgate.net/profile/Ahmed-Gomaa-31/publication/369900140_STRENGTHENING_OF_CORRODED_REINFORCED_CONCRETE_BEAMS_EXPOSED_TO_TORSIONAL_AND_FLEXURAL_STRESSES/links/64320ea220f25554da1b52f6/STRENGTHENING-OF-CORRODED-REINFORCED-CONCRETE-BEAMS-EXP.
[6] S. Kinnunen and H. Nylander, *Punching of concrete slabs without shear reinforcement*. Elander New York, 1960.
[7] E. M. Lotfy, A. M. Gomaa, S. Hosny, A. Sherif, and M. A. Ahmed, "Predicting of Punching Shear Capacity of Corroded Reinforced Concrete Slab-column Joints Using Artificial Intelligence Techniques," doi: 10.4186/ej.20xx.xx.x.xx.
[8] A. M. Gomaa *et al.*, "Comparative study of models predicting punching shear capacity of strengthened corroded RC slab- column joints," *HBRC J.*, vol. 20, no. 1, pp. 257–274, 2024, doi: 10.1080/16874048.2024.2310936.
[9] C. E. Broms, "Concrete flat slabs and footings: Design method for punching and detailing for ductility," KTH, 2005.
[10] J. Di Stasio, "Transfer of bending moment between flat plate floor and column," in *Journal Proceedings*, 1960, vol. 57, no. 9, pp. 299–314.
[11] C.-C. Chen and S.-L. %J A. S. Chen, "Strengthening of reinforced concrete slab-column connections with carbon fiber reinforced polymer laminates," vol. 10, no. 1, p. 265, 2019.
[12] L. Shen, Y. Shen, and S. Liang, "Reliability Analysis of RC Slab-Column Joints under Punching Shear Load Using a Machine Learning-Based Surrogate Model," *Buildings*, vol. 12, no. 10, 2022, doi: 10.3390/buildings12101750.
[13] A. Muttoni, "Punching shear strength of reinforced concrete slabs without transverse reinforcement," *ACI Struct. J.*, vol. 105, no. 4, pp. 440–450, 2008, doi: 10.14359/19858.
[14] L. Wu, T. Huang, Y. Tong, and S. %J B. Liang, "A Modified Compression Field Theory Based Analytical Model of RC Slab-Column Joint without Punching Shear Reinforcement," vol. 12, no. 2, p. 226, 2022.
[15] P. Chetchotisak, P. Ruengpim, D. Chetchotsak, and S. Yindeesuk, "Punching Shear Strengths of RC Slab-Column Connections: Prediction and Reliability," *KSCE J. Civ. Eng.*, vol. 22, no. 8, pp. 3066–3076, 2018, doi: 10.1007/s12205-017-0456-6.
[16] H. D. Nguyen, G. T. Truong, and M. %J E. S. Shin, "Development of extreme gradient boosting model for prediction of punching shear resistance of r/c interior slabs," vol. 235, p. 112067, 2021.
[17] S. Mangalathu, H. Shin, E. Choi, and J.-S. %J J. of B. E. Jeon, "Explainable machine learning models for punching shear strength estimation of flat slabs without transverse reinforcement," vol. 39, p. 102300, 2021.
[18] A. A. Manar and T. M. Mansour, "Modelling of Shear Strength for Reinforced Concrete Beams Provided with Side-Face Reinforcement in Dependence of Crack Inclination Angle," vol. 4, no. 6, 2019.
[19] H. Erdem, "Prediction of the moment capacity of reinforced concrete slabs in fire using artificial neural networks," *Adv. Eng. Softw.*, vol. 41, no. 2, pp. 270–276, 2010, doi: 10.1016/j.advengsoft.2009.07.006.
[20] S. Mangalathu, H. Jang, S. H. Hwang, and J. S. Jeon, "Data-driven machine-learning-based seismic failure mode identification of reinforced concrete shear walls," *Eng. Struct.*, vol. 208, no. January, p. 110331, 2020, doi: 10.1016/j.engstruct.2020.110331.
[21] S. Mangalathu and J.-S. Jeon, "Machine Learning–Based Failure Mode Recognition of Circular Reinforced Concrete Bridge Columns: Comparative Study," *J. Struct. Eng.*, vol. 145, no. 10, 2019, doi: 10.1061/(asce)st.1943-541x.0002402.
[22] V. L. Tran and S. E. Kim, "A practical ANN model for predicting the PSS of two-way reinforced concrete slabs," *Eng. Comput.*, vol. 37, no. 3, pp. 2303–2327, 2021, doi: 10.1007/s00366-020-00944-w.
[23] H. Akbarpour and M. Akbarpour, "Prediction of punching shear strength of two-way slabs using artificial neural network and adaptive neuro-fuzzy inference system," *Neural Comput. Appl.*, vol. 28, no. 11, pp. 3273–3284, 2017, doi: 10.1007/s00521-016-2239-2.
[24] K. K. Choi, M. M. Reda Taha, and A. G. Sherif, "Simplified punching shear design method for slab-column connections using fuzzy learning," *ACI Struct. J.*, vol. 104, no. 4, pp. 438–447, 2007, doi: 10.14359/18774.
[25] F. Ahmadkhanlou and H. Adeli, "Optimum cost design of reinforced concrete slabs using neural dynamics model," *Eng. Appl. Artif. Intell.*, vol. 18, no. 1, pp. 65–72, 2005, doi: 10.1016/j.engappai.2004.08.025.
[26] S. Guandalini, O. L. Burdet, and A. Muttoni, "Punching tests of slabs with low reinforcement ratios," *ACI Struct. J.*, vol. 106, no. 1, pp. 87–95, 2009, doi: 10.14359/56287.
[27] A. M. Gomaa, E. M. Lotfy, S. A. Khafaga, S. Hosny, and M. A. Ahmed, "Experimental , numerical , and theoretical study of punching shear capacity of corroded reinforced concrete slab-column joints," *Eng. Struct.*, vol. 289, no. May, p. 116280, 2023, doi: 10.1016/j.engstruct.2023.116280.
[28] Y. Tian, "Behavior and Modeling of Reinforced Concrete Slab-Column Connections," p. 210, 2007.
[29] M. Zhang, M. Deng, Z. Wu, and J. Pan, "Flexural cracking behavior and calculation approach of reinforced highly ductile fiber-reinforced concrete beams," *Arch. Civ. Mech. Eng.*, vol. 21, no. 4, pp. 1–14, 2021, doi: 10.1007/s43452-021-00309-0.
[30] M. A. L. Silva, J. C. P. H. Gamage, and S. Fawzia, "Performance of slab-column connections of flat slabs strengthened with carbon fiber reinforced polymers," *Case Stud. Constr. Mater.*, vol. 11, p. e00275, 2019, doi: 10.1016/j.cscm.2019.e00275.
[31] K. Qian, J. S. Li, T. Huang, Y. H. Weng, and X. F. Deng, "Punching shear strength of corroded reinforced concrete slab-column connections," *J. Build. Eng.*, vol. 45, no. August 2021, p. 103489, 2022, doi: 10.1016/j.jobe.2021.103489.
[32] E. M. Golafshani and A. Ashour, "A feasibility study of BBP for predicting shear capacity of FRP reinforced concrete beams without stirrups," *Adv. Eng. Softw.*, vol. 97, pp. 29–39, 2016, doi: 10.1016/j.advengsoft.2016.02.007.
[33] H. Naderpour and M. Mirrashid, "An innovative approach for compressive strength estimation of mortars having calcium inosilicate minerals," *J. Build. Eng.*, vol. 19, no. March, pp. 205–215, 2018, doi: 10.1016/j.jobe.2018.05.012.
[34] M. H. Ilkhani, H. Naderpour, and A. Kheyroddin, "A proposed novel approach for torsional strength prediction of RC beams," *J. Build. Eng.*, vol. 25, p. 100810, 2019, doi: 10.1016/j.jobe.2019.100810.
[35] V. L. Tran, D. K. Thai, and S. E. Kim, "Application of ANN in predicting ACC of SCFST column," *Compos. Struct.*, vol. 228, no.

April, p. 111332, 2019, doi: 10.1016/j.compstruct.2019.111332.
[36] P. Adebar, J. G. Mutrie, R. DeVall, and D. Mitchell, “Seismic design of concrete buildings: The 2015 Canadian building code,” *NCEE 2014 - 10th U.S. Natl. Conf. Earthq. Eng. Front. Earthq. Eng.*, 2014, doi: 10.4231/D39W09032.
[37] A. C. I. Committee, “ACI 318-19: Building Code Requirements for Structural Concrete and Commentary,” *Am. Concr. Inst. Farmingt. Hills, MI, USA*, 2019.